ICARUS **133,** 36–68 (1998)
ARTICLE NO. IS985920

Simulation of the Formation and Evolution of the Perseid Meteoroid Stream

P. Brown and J. Jones

Department of Physics and Astronomy, University of Western Ontario, London, Ontario, N6A 3K7, Canada
E-mail: peter@danlon.physics.uwo.ca

Received October 6, 1997; revised January 30, 1998

Four major models of cometary meteoroid ejection are developed and used to simulate plausible starting conditions for the formation of the Perseid stream. In addition to these physical variants, three different choices for initial meteoroid density (100, 800, and 4000 kg m^{-3}) are used to produce a total of 12 distinct initial models. The development and evolution of the stream are simulated for each model by ejecting 10^4 test meteoroids at seven distinct mass categories over the full arc of 109P's orbit inside 4 AU at each perihelion passage from 59 to 1862 AD. All test meteoroids are followed to their descending nodes for times closest to the recent perihelion passage of 109P (1992). In addition to these integrations, we have also performed long-term integrations over the interval from 5000 to 10^5 years ago using two plausible sets of starting orbits for 109P over this interval.

We find that the choice of cone angle and precise cutoff distance for ejection make only minor modifications to the overall structure of the stream as seen from Earth. The assumed density for the meteoroids has a major influence on the present activity of the stream as radiation pressure moves nodal points further outside Earth's orbit and hence decreases the probability of delivery for lower density meteoroids. The initial ejection velocities strongly influence the final distributions observed from Earth for the first ~5 revolutions after ejection, at which point planetary perturbations and radiation effects become more important to subsequent development. The minimum distance between the osculating orbit of 109P at the epoch of ejection and the Earth's orbit is the principal determinant of subsequent delivery of meteoroids to the Earth.

The best fit to the observed present flux location and peak strengths are found from models using Jones (1995) ejection velocity algorithm with an $r^{-0.5}$ dependence and densities between 0.1 and 0.8 g cm^{-3}.

The recent activity outburst maxima observed for the Perseids from 1989 to present show a systematic shift in location from year to year, which is explained by changing ages of the primary component of the meteoroids making up the outbursts. Specifically, it is found that from 1988 to 1990 ejecta from 1610 and 1737 are the dominant population, while 1862 and 1610 are the primary material encountered in the outbursts from 1991 to 1994. From 1995 to 1997 the most prevalent populations are ejections from 1479 and 1079. The older populations tend to shift the locations of the maximums to higher solar longitudes. A discrepancy which is present for both the 1993 and 1994 peak locations of 1–2 h between the observed and modeled flux profiles is most likely the result of emissions from 1862, which were observed to have a large component of their velocity out of the cometary orbital plane.

The cause of Perseid activity outbursts is found to be direct planetary gravitational perturbations from Jupiter and Saturn that shift the nodes of stream meteoroids inward and allow them to collide with Earth. The last such perturbations was due to Jupiter in 1991, and this effect combined with the return of 109P in 1992 produced the strong displays from 1991 to 1994.

On average, it is found that the Perseids observed each year in the core portion of the stream left the parent comet (25 ± 10) $\times$ 10^3 years ago. From the modeling, the total age of the stream is estimated to be on the order of 10^5 years. From the simulations over the last 2000 years, the progression rate of the node of the stream is estimated at (2.2 ± 0.2) $\times$ 10^{-4} degrees/annum.

The effect of terrestrial perturbations has been evaluated from the long-term integrations and found to play only a minor role in the stream's development, producing a 5–10% increase in the stream's nodal and radiant spread as compared to an identical simulation without the Earth.

The primary sinks for the stream are found to be hyperbolic ejection due to Jupiter (and to a smaller degree Saturn) as well as attainment of sungrazing states. Both the relative and absolute contributions of these two loss mechanisms to the decay of the stream is found to be highly dependent on the assumed cometary starting orbits, with as much as 35% of initially released stream meteoroids removed by hyperbolic ejection after 10^5 years for the smallest Perseids on some starting orbits to less than 1% removed after the same time for larger meteoroids on other potential seed orbits. On average, it requires 40–80 $\times$ 10^3 years for a noticeable fraction of the initial population (>0.1%) to be removed by these mechanisms, depending on the chosen starting orbits. © 1998 Academic Press

Key Words: Perseids; meteoroids; numerical integration.

1. INTRODUCTION

The recovery of Comet 109P/Swift–Tuttle in 1992 marked the beginning of an intensive effort to characterize

0019-1035/98 $25.00

one of the largest known Earth-crossing bodies. Much has been learned of Swift–Tuttle in the intervening years (cf. Yau *et al.* 1994), but the comet's equally famous trail of meteoroidal debris remains mysterious. The return of the comet was presaged by a strong increase in activity from the Perseids beginning most notably in 1991 (Brown and Rendtel 1996). This marked the first occasion when a large change in the flux of the shower was unambiguously recorded. Indeed, Olivier (1925) comments that "...the Perseids appear with no remarkable variations in numbers practically every August."

The Perseid shower has been recognized in the sky almost as long as records of such phenomena have been kept. Hasegawa (1993) has traced ancient records of the stream back 2000 years and it seems probable that the stream is older still. Detailed observational histories of the stream have been given by Kronk (1988) and Rendtel *et al.* (1995). The shower is also notable as the first instance in which a comet was definitively linked to a meteor shower, this connection was made by Schiaparelli (1867).

The first attempts to understand the stream in an analytical form were those of Twining (1862) who investigated the perturbing effects of the Earth on Perseid meteoroids and found no sensible perturbations from this mechanism. Further research through the late nineteenth and early twentieth century concentrated on interpreting visual observations of the shower. Throughout this period there was general understanding that comets and meteoroid streams were linked, the weight of opinion being that the latter originated from the former, but contrary views were not uncommon. Whether meteoroids were continually discharged or periodically released from comets remained unclear.

Progress in understanding the stream relied heavily on the untangling of the cometary–meteoroid decay process highlighted by Guigay (1947) who postulated that the stream was formed entirely by a collision between a proto Swift–Tuttle and another body. The resulting spall accounted for the Perseids and at least five other comets noted by Guigay to have relatively close orbital intersections. Kresak (1957) pointed out the numerous difficulties in this interpretation and its contradiction to the mounting photographic meteor data then available for the stream.

Hamid (1951) was the first to model the ejection of the meteoroids from Swift–Tuttle using Whipple's (1951) "icy-snowball" cometary model and analytically follow the resulting orbits under the effects of secular planetary perturbations. He noted that the formation and subsequent evolution of the stream is intimately linked with the past history of the comet, which he determined through secular perturbations of the then best-available orbit for Swift–Tuttle. The variation in orbital elements for Perseid meteoroids was found to be in general agreement with photographic data, assuming ejection velocities on the order of 10 m/s, and the age of the stream was determined to be 40,000 years.

Southworth (1963) performed a more detailed analysis of the evolution of the stream by computing numerically the gravitational perturbations on individual stream meteoroids instead of mean perturbations from secular theory. He found that the variation observed in the radiant position and velocities of meteoroids in the stream implied scattering much stronger than planetary perturbations alone could explain. Using similar ejection velocities as Hamid, he concluded that either strong nongravitational effects out of the orbital plane were at work or the stream was formed not through gradual disintegration of the parent comet but rather by way of a single, large cometary explosion (citing Guigay's (1947) hypothesis) approximately 1000 years ago. His work implied an upper limit of 6000 years for the age of the stream.

Sekanina (1974) investigated the dynamics of the Perseid stream based on a detailed consideration of the likely ejection conditions from the parent comet and the effects that variations in these conditions, such as location and direction of ejection, might make on the final meteoroid distributions. By examining ancient records of recorded appearances of the Perseids, he concluded that a systematic variation in the time of recorded Perseid returns relative to the perihelion passage of the comet suggested that the meteoroid emission lasted for several months, probably beginning shortly before perihelion and implicitly assumed to be nearly continuous during this time. In particular, he suggested that the comet may vary its dust output dramatically from apparition to apparition, resulting in preferential locations for strong Perseid returns relative to the comet's perihelion passage and the initial emission epoch.

The concept that the Perseid stream was formed by emission of meteoroids at a single location along the orbit of Swift–Tuttle was further developed by Katasev and Kulikova (1975). Using a variety of ejection locations and velocities, they determined the best agreement between computed orbits from an isotropically emitting Swift–Tuttle, and the observed stream was found by using velocities of 100 m/s and an ejection centered at 30° true anomaly. No account of subsequent planetary perturbations or the past history of the comet was employed and the fit relied entirely on the veracity of the orbital elements for the stream presented by Southworth (1963).

The failure of Swift–Tuttle to return in 1981 as predicted, based on the 1862 orbital solution alone, was the most significant development in the understanding of the stream to that time. It became clear that our ideas about Swift–Tuttle based on the 1862 observations of the comet alone were in error and along with them previous attempts to understand the stream. The recovery of 109P/Swift–Tuttle in 1992 provided hope that serious attempts to understand the stream might be successful as the complete history of

Swift–Tuttle's orbital evolution over the past 2000 years was then possible.

Wu and Williams (1993) have used Whipple's ejection model in conjunction with a Monte Carlo approach to model the behavior of 500 test meteoroids of the same mass ejected during the 1862 passage of Swift–Tuttle. They conclude that gravitational perturbations from the planets move the original non-Earth intersecting orbits into Earth-crossing paths, and they suggest that much of the recent intense activity from the Perseids is from 1862 ejecta, further suggesting that 1994 would be the culmination of this activity. Use of small numbers of test particles of only one mass and an older orbit for Swift–Tuttle limit the generality of their results. To improve on this early model, Williams and Wu (1994) used a better orbit for the comet and a distribution of masses to make quantitative predictions concerning activity for the Perseids in the early 1990s as well as locations for the maximum of the shower in each year from 1988 to 1995. The results still suggested that peak activity would occur in 1994, but the predicted times for maximum were consistently 2 h earlier than observed.

Harris and Hughes (1995) have investigated the distribution of semimajor axes of photographic Perseid meteoroids. They find no variation as a function of mass and conclude that the final ejection velocities for Perseid meteoroids are independent of mass and all of relatively high velocity. This result will be discussed in detail in Section 2. Harris *et al.* (1995) expanded upon this result by modeling the ejection of Perseids using a Maxwellian velocity distribution centered about 0.6 km/s. Through integration of 109P/Swift–Tuttle backward for 0.16 Ma, they also simulated formation of the stream as a whole, taking ejections from the comet every 5000 years without accounting for planetary perturbations or radiation forces. They conclude that the stream is roughly 160,000 years old.

Here we present a detailed numerical model for the formation and subsequent evolution of the Perseid stream. In Section 2 we discuss the best available information concerning the initial conditions for the formation of the stream, including the cometary orbit as a function of time and the meteoroid ejection process. In Section 3, our various model choices for initial conditions are described and the modeling process is discussed along with our integrator used to simulate the effects of perturbations to the present time on stream meteoroids. Results of these numerical experiments are presented in Section 4, and discussion of the major effects governing the development of the stream are given in Section 5. We summarize our results and major conclusions in Section 6.

From our analysis, we will attempt to gain some understanding of several key questions, such as:

1. How do the initial ejection conditions assumed affect the final observed distributions and over what time scales are the initial ejection conditions "erased" due to radiation forces and planetary perturbations? In particular, are the final distributions sensitive to the assumed cone angle over-which ejections take place, the largest distance from the Sun the meteoroids are ejected, and the assumed density of the meteoroids? What changes in the final distributions are a function of mass? What is the best model representation of the ejection process? What is the range of initial ejection velocities?

2. Why has the position of the outburst peak of the Perseids observed over the past decade changed position in the stream? Why has the outburst portion of the stream also varied in intensity so much in this time interval? Why did this recent outburst activity "turn on" so quickly in 1991? What are the underlying causes of the outbursts—intrinsic changes in the dust output of the comet in the past, the recent passage of Swift–Tuttle, or some other effect?

3. What ejection(s) contribute most to the outburst activity we have seen in the stream over the past decade? Are most of these meteoroids from the 1862 passage of the comet as has been widely assumed?

4. What is the age of the main core of the Perseid stream? What is the ultimate age of the stream?

5. What is the current progression rate of the node of the stream?

6. What effect does the Earth have on the longer term development of the stream?

7. What are the mechanisms that remove meteoroids from the stream and over what time scales do they act?

8. What controls the delivery of Perseid meteoroids to Earth?

2. INITIAL CONDITIONS: THE COMETARY DECAY PROCESS

2.1. Physical Models

Stream meteoroids are ejected from comets. As comets approach the Sun, the number of meteoroids ejected from a comet tends to increase as does the magnitude of the ejection velocity. The ejection velocity is a small fraction of the orbital velocity of the comet and hence the daughter meteoroids move along similar orbits to the parent comet. Sublimating volatiles (primarily water–ice) are responsible for the release of particles through momentum exchange with the meteoroid grains.

The preceding paragraph summarizes those general aspects of the meteoroid ejection process for which there is near unanimous agreement by workers in the field. Adding additional details to the preceding picture, particularly quantitative ones, requires interpretation of often contradictory observational and theoretical aspects of the cometary ejection process. Remarkable as it seems, this picture is almost identical to the one first presented by Whipple

(1951). The only major change from that early model which might be widely accepted today is the observational fact that the active regions of comets (and hence the areas where meteoroids might be ejected) are small fractions of the total surface area of the comet and thus dust is initially confined to jets immediately after leaving the nucleus surface (cf. McDonnell *et al.* 1987). At great distances from the nucleus, however, the meteoroids in such jets tend to spread out into larger cones, and the final physical picture may not be very different from Whipple's (cf. Jones 1995).

To try to model the evolution of a meteoroid stream, the process by which the stream initially formed is of considerable interest. Whether the initial formation process determines the ultimate character of the stream (in comparison to planetary perturbations or radiation forces) is not clear and may vary from stream to stream. Since uncertainty exists about the formation process, we choose to use several different models of formation along with wide variations for those parameters which we feel are particularly poorly known to determine just how strongly the initial conditions affect the final results. In the end, each model and set of parameter choices lead to a range of possible values for one crucial number, namely, the final ejection velocity of the meteoroid relative to the comet. Knowing this value and the location of ejection, comet orbit and meteoroid shape permits forward integration of the equations of motion for the stream meteoroid and some approximate estimate of its future location.

As it is impossible to make a rigorous determination of the precise location of ejection for a meteoroid, a Monte Carlo approach must be employed. Here we assume that meteoroids are ejected at random values of true anomaly over the arc of the 109P/Swift–Tuttle's orbit inside 4 AU in numbers proportional to the amount of solar energy received by the nucleus. That meteoroids would be ejected with equal probability for all values of true anomaly (for 109P, between $303° < \nu < 120°$) under these assumptions was first noted by Kresak (1976). This result is due to the r^{-2} variation of solar flux and the $r^2\ d\nu/dt$ constant of motion from Kepler's second law removing the effects of changes in ν on the meteoroid production function. The idea that ejection occurs inside 4 AU for 109P/Swift–Tuttle has been constrained partially by the observations of Boettnhardt *et al.* (1996) and O'Ceallaigh (1995) who observed little or no coma in Swift–Tuttle at 5 AU during its 1992 apparition. While water production is usually taken to cease near 3 AU (cf. Festou *et al.* 1993), some more distant production is commonly observed in many comets and we chose 4 AU as a compromise, acknowledging that much of this distant production is due to more volatile compounds than water. We will investigate the effects on the observed stream of choosing still smaller cutoffs in solar distance for meteoroid production in Section 4.

The orbit of 109P/Swift–Tuttle has been determined with accuracy backward nearly 2000 years. Marsden *et al.* (1993) and Yau *et al.* (1994) used observations from the 1992 perihelion passage along with older observations extending back to 69 BC to reverse integrate the equations of motion of the comet. Their independently derived results agree to high precision. We use the orbits given in Yau *et al.* (1994) as the initial seed orbits for all models, noting that the slight difference between the ephemera is much smaller than other uncertainties in our adopted models.

The shape (more precisely cross-sectional area to mass ratio) of the meteoroids comes into play not only during the ejection process but also in the particles' subsequent evolution under radiation forces. Gustafson (1989) has noted the large variation in ejection velocity predicted solely on the basis of modest variations in shape factor for meteoroids. Similar work by Nakamura *et al.* (1994) supports the notion that shapes other than the idealized sphere would tend to have higher ejection velocities. We discuss our attempts to account for this effect in Section 3. The effect of shape on radiation pressure is significant only for the smallest of meteoroids considered here and is discussed further in Section 3.

Past attempts to model meteoroid streams (cf. Williams 1993 for a review) have relied almost entirely on the Whipple model and the numerical relation he determined assuming gas drag lifts a spherical meteoroid away from the sunward side of the nucleus, namely

$$V_{\text{eject}} = 8.03 r^{-1.125} \rho^{-1/3} R_c^{1/2} m^{-1/6} f, \tag{1}$$

where R_c is the radius of the cometary nucleus, ρ is the bulk density of the meteoroid, m is the mass of the meteoroid, f is the fraction of incident solar radiation used in sublimation, r is the heliocentric distance in AU, and V_{eject} is the final grain ejection velocity relative to the nucleus in ms^{-1}. A typical value of these parameters ($R_c = 5$ km, $\rho = 800$ kg m^{-3}, $f = 1$, and $m = 0.1$ g) results in a V_{eject} of 36 ms^{-1} at 1 AU. Note that we have ignored the gravitational attraction of the nucleus in (1). We set $f = 1$ throughout.

Indeed, the Whipple ejection formula provides the starting point for much of the modeling we perform. The shortcomings of the Whipple model, namely assumption of blackbody-limited nucleus temperature (instead of temperature limited) and the neglect of the adiabatic expansion of the gas have been corrected by (among others) Jones (1995) and we use his revised Whipple formula

$$V_{\text{eject}} = 10.2 r^{-1.038} \rho^{-1/3} R_c^{1/2} m^{-1/6} \tag{2}$$

for our basic model. In particular, the Whipple formulation ignores the role of isolated jets of activity, which is taken into account in the Jones' model. Despite the modifica-

tions, the Jones' equation is very close to that of the original Whipple model. We examine the effects of changes in ejection cone angle (the angle between the solar-direction and velocity vector) to the final results in Section 4.

Of the parameters in the Jones' formula, the radius of the nucleus is most certain in the case of 109P/Swift–Tuttle. From visible observations of the bare nucleus, Boehnhardt *et al.* (1996) conclude that the nucleus has a radius of 11.2 ± 0.3 km, while O'Ceallaigh *et al.* (1995) found the nuclear radius to be 11.8 ± 0.2 using similar observations. Fomenkova *et al.* (1995) derived a radius of 15 ± 3 km from observations in the IR. These extremely large radius estimates are consistent with the apparent lack of nongravitational forces needed to explain Swift–Tuttle's motion over the past two millennia (Yau *et al.* 1994). We adopt a radius of 10 km throughout and note that this is almost twice the mean nuclear radius of Halley.

Theoretical models are no better than the assumptions on which they are based and if we ignore for the moment the details of the models, we see that they agree on many of the parameters which govern the speed of ejection of the meteoroids. Of particular interest to us is the variation of the ejection speed with the Sun–comet distance. Both the Whipple-derived theories and most other models predict that the variation should be of the form

$$V \propto r^n. \tag{3}$$

For the Whipple-like theories, n is close to -1, while from observations of coma ejections/halo expansions (cf. Whipple 1980, Combi 1989), n is close to -0.5. While there can be much discussion on theoretical grounds as to what is the most appropriate value to adopt in practice, at this stage of the process we chose to investigate both possibilities and to make the final choice on the basis of which best described the observed activity of the stream.

Another shortcoming of the Whipple approach is its assumption that all sublimation is confined to the nucleus surface and is the sole source for gas in the coma. Data gathered during the Halley fly-bys in particular have suggested that sublimation occurs throughout the coma as active grains continue evaporating and releasing H_2O. This contention is supported by the observation that cometary coma gas distributions tend to be spherical despite the presence of jets of activity, that the near-nucleus brightness of the coma drops off slower than $1/r^2$ as expected for surface production away from the surface and that the terminal dust grain velocity inferred from cometary tail observations shows a weak mass dependence, suggesting fragmentation of large grains far from the nucleus might be the source for many of the smaller grains. This concept of "distributed" production in the coma is not new, but recently Crifo (1995) has incorporated the concept of distributed production into a general physicochemical model of the inner coma along with detailed numerical results of the resulting effects on the terminal dust velocity as a function of mass. He finds that dust ejection velocities for a given mass are broad distributions that tend to have velocity peaks lower than the "classic" surface production models as compared to the single-valued velocities derived from the Whipple model. Steel (1994) has emphasized the need to incorporate this effect in the cometary coma into meteor stream modeling, but to date this has not been done.

2.2. Constraints from Meteor Data

Recently, Harris and Hughes (1995) examined photographic meteor data in an attempt to use such information to constrain the cometary ejection process for the Perseids. In particular, their work (as well as that of Williams (1996)) has concentrated on the distribution of semimajor axes of stream meteoroids. These authors suggest that if no substantial planetary perturbations affect a meteoroid, it is possible to use the true semi-major axis of the particle along with assumed distributions of ejection directions and locations along the cometary orbit to constrain the ejection velocity of the meteoroids. Indeed, Harris and Hughes (1995) found that there is no variation in the semi-major axis distribution with meteoroid mass and conclude that all meteoroids reach essentially the same final velocity independent of mass. By comparing the observed distributions of semimajor axes to trial distributions, they suggest that this velocity is close to the final Maxwellian gas velocity, about 0.6 km/s for Swift–Tuttle at perihelion.

In using the photographic data of the stream compiled from more than a half dozen different surveys, the effects of measurement errors have not been discussed in detail by either Harris and Hughes (1995) or Williams (1996).

These data consist of Perseid orbits derived from the photographic data bases of the IAU Meteor Data Centre (Lindblad 1991). To find a value for a (semimajor axis) from photographic observations, the original heliocentric velocity must be determined. In measuring the atmospheric velocity, however, a number of possible errors may be encountered, among them:

1. The measured velocity in the atmosphere must be corrected for deceleration of the meteoroid over the course of the length of the trail, but this can only be done in an approximate manner. Older observations have used the classic $dv/dt = a + bt + ce^{kt}$ empirical velocity correction (Jacchia and Whipple 1961) whose validity is questionable and yields results different from modern applications of methods to account for deceleration such as the gross-fragmentation model for large meteoroids of Ceplecha *et al.* (1993).

2. For short trails, the number of measured points may be limited and the resulting velocity uncertain. This is

particularly a problem with Perseids which tend to have very short-lived trails in the atmosphere.

3. Wake, fragmentation, and flares along the trajectory may make measurement of the trail breaks difficult.

4. Instrumental effects, particularly related to the frequency of the shutter, can lead to systematic errors. Such effects have recently been found (and removed) from the photographic observations of the Lost City fireball (Ceplecha 1996).

The same photographic data bases used by the previous authors have been examined in detail by Kresakova (1974) and Porubcan (1977) in relation to the Perseids. They have shown that among the dozen major photographic surveys, the intersurvey deviations of the rms intrasurvey variation in the measured heliocentric velocity for Perseid meteoroids (which is approximately 41 km/s at 1 AU) varies from 0.3 km/s to more than 2.0 km/s, with the majority greater than 1 km/s. At 1 AU, the measured heliocentric velocity is related to the semimajor axis via

$$V_h^2 = GM\left(2 - \frac{1}{a}\right), \tag{4}$$

where G is the universal gravitational constant, M is the mass of the Sun, and V_h is the heliocentric velocity in terms of the circular velocity at 1 AU. Fractional errors in velocity translate into very large errors in a, especially for large values of a (such as the Perseid stream orbit). More precisely,

$$\frac{da}{a} = 4a\left[\frac{dV_h}{V_h}\right], \tag{5}$$

which implies that the smallest rms intrasurvey deviations in V_h for the Perseids corresponds to error dispersions in a of nearly 100%. The bulk of the data have much higher errors, which would be expected to push a beyond the hyperbolic limit. In fact, nearly 1/3 of all available Perseid orbits are at or beyond the parabolic limit, though none of these are seriously considered hyperbolic.

The conclusion for the Perseids is that the distribution of semimajor axes observed by even the most sensitive techniques currently available still produces no useful information concerning the initial conditions of ejection of the stream meteoroids. A similar conclusion has recently been reached by Kresak (1992).

While semimajor axis distributions are prone to large errors masking original ejection velocity information for the Perseids, geocentric radiant distributions and flux information for the stream do not suffer as greatly. Indeed, such information provides the basis for interpretation and validation of the results of our modeling and help to discriminate the most probable initial conditions for the ejection of Perseid meteoroids. These data are presented in Section 4 along with a discussion of the model results.

3. THE MODEL

3.1. Initial Ejection Models: Overview

From the forgoing discussion, it is clear that an ejection model of the classic-Whipple type alone does not cover the many possible important variations in ejection conditions that current observational data and theoretical modeling suggests are possible. As the differences in the final meteoroid distributions may be sensitive to the initial model choices, it is desirable to use several different ejection schemes and compare the final results. The resulting differences will determine which models are best able to fit the available Perseid observations, assuming the intermodel differences are great enough to distinguish the outcomes.

After reviewing the available information on the cometary ejection process as summarized in Section 2, we have decided to use four major models of ejection of meteoroids from 109P/Swift–Tuttle.

The first model uses the results of Crifo's (1995) coma modeling for distributed production in the coma. His result for the average terminal velocity of the dust (appropriate for grains from 10 cm $< s < 10^{-4}$ cm) for olivine grains as a function of grain radius, s, can be expressed empirically as

$$\log_{10}(V_{\text{eject}}) = -2.143 - 0.605 \log_{10} s \tag{6}$$

and we assume the production varies with heliocentric distance as $r^{-0.5}$. The result is scaled from his simulation work (which was designed for Halley to compare the final results with Giotto measurements) to that appropriate for 109P/Swift–Tuttle, assuming the same fractional area on both comets were active. This value for the average velocity (V_{eject}) is then used along with Crifo's distributions for the differential flux as a function of velocity for a mass of 10^{-2} g, which has an empirical form of

$$P(V - V_{\text{eject}}) = \frac{1}{e^{3.7}} \exp\left[\frac{3.7 - 10.26(V - V_{\text{eject}}) + 4.12(V - V_{\text{eject}})^2}{1 - 1.03(V - V_{\text{eject}}) + 0.296(V - V_{\text{eject}})^2}\right], \tag{7}$$

where $P(V - V_{\text{eject}})$ is the probability of finding a grain with ejection velocity V. This is Model 1.

The second model is the Jones modification to the original Whipple formula with the exception that the solar distance dependence on the ejection velocity is taken to be $r^{-0.5}$. We call this variant Model 2.

As the Whipple model has been used by almost all previous workers in modeling streams, it seems appropriate for comparison of our final results to past results to include this model. The slight modification to the Whipple model by Jones is used and we call this Model 3 throughout. It is similar to 2 except that the heliocentric velocity dependence is $r^{-1.038}$.

The fourth and last model uses the same ejection velocity formulation as Model 3, with the exception that it is not a single-valued function for a given choice of input parameters. Instead, we use a parabolic distribution centered about the nominal Jones velocity in an attempt to account for the different ejection velocities for a given mass due to the differing shape factors. Since we have no numerical constraints a priori regarding grain shapes, we use this parabolic distribution in an attempt to account for this variation. This is Model 4.

For each model, the absolute value for the grain ejection velocity will vary as a function of the chosen density. Estimates for cometary nucleus densities vary widely, with evidence from Halley suggesting values in the ~100 kg m^{-3} range (Rickman 1986) or lower, while Sagdeev *et al.* (1987) estimate this value to be closer to ~600 kg m^{-3}. However, the nucleus density may have little relationship to the density of smaller grains. Indeed, Ceplecha (1988) and Verniani (1973) have analyzed fireball and radio meteor sized bodies (10^5–10^{-4} g) and find bulk densities near 800 kg m^{-3}. In contrast, Babadzhanov (1993) finds densities closer to ~4000 kg m^{-3} from photographic meteor data and application of a fragmentation model to the observed data. These wide ranges for the possible densities of Perseid meteoroids have led us to adopt three distinct densities we use for all models, namely 100, 800, and 4000 kgm^{-3}, which we enumerate as 1, 2, and 3 model variants. Thus, the distributed production model with meteoroids of density 100, 800, and 4000 kgm^{-3} are referred to as Models 11, 12, and 13, respectively. The ejection velocity formula for each model is given in Table I, and sample distributions for ejection velocities as a function of heliocentric distance are shown in Fig. 1 for Perseid meteoroids of mass 10^{-2} g.

We have taken the meteoroid mass to be the independent variable and plot all results in terms of initial ejection mass. In total, we have 12 distinct model variants and for each we eject 10,000 test meteoroids at differing masses from 10^{-5}–10 g for each perihelion passage of 109P/Swift–Tuttle. We have used 61 mass categories over this mass range for the 1862 and 1737 passages of the comet for each model variant—each mass category is 0.1 greater in log ($M(g)$) than the previous category. This implies that a total of 610,000 test meteoroids are ejected for each model variant for each passage (1862 and 1737), totaling 7.32×10^6 particles. For passages from 59 to 1610 AD, only 7 mass categories are used over the full mass range due to computational limitations, each 10 times greater than the previous (1.0 in log ($M(g)$)) totaling 8.4×10^5 meteoroids per perihelion passage.

For each model variant, the same basic Monte Carlo approach is taken to determine the point of ejection and ejection velocity/direction. As described in Section 2, the point along the orbit of 109P/Swift–Tuttle where ejection occurs is chosen randomly from within the true anomaly range from $303° < \nu < 120°$ or $r < 4$ AU. After this ejection point is determined, the appropriate ejection speed is then found, depending on the model variant, using one of the formulas given in Table I. The direction of ejection is confined to the sunward side of the comet and is chosen randomly, while the final ejection magnitude is calculated according to each model formula. As the direction of ejection is stored in the final data file, it is possible to select meteoroids ejected from within any sized cone angle (the angle measured from the sun-line direction to the outer limit of the allowed ejection directions) a posteri and study the final distributions. The resulting cometocentric velocity is added to the cometary velocity at the ejection location to derive the initial orbit. This process is repeated for all 10,000 meteoroids for a particular run and this file is then used as the input to the numerical integrator.

3.2. *The Numerical Integrator*

The basic form of the numerical integrator uses an RK4 architecture with variable step size. An early version of this integrator was described by Jones (1985). This integrator has been specifically designed for integrating large numbers of bodies as quickly as possible over (relatively) short solar system times. Whereas typical integrators used in solar system work such as RADAU (Everhart 1985) or SWIFT (Levison and Duncan 1994) are designed for high precision and long periods of integration, we are concerned with maintaining only modest precision and concentrating instead on particle throughput.

To this end, the integrator uses a simple RK4 numerical integration scheme adapted from Press *et al.* (1986). The basic step size (h) was chosen initially based on numerical experiments offsetting speed and accuracy—a typical value being 0.01 years. For an orbit as eccentric as 109P/Swift–Tuttle, variable step-size routines we tested suggested that the large number of steps near perihelion did not increase the overall orbital accuracy (our primary interest) and that the resulting numerical round-off errors and loss of speed were significant. Jones (1985) found that an empirical formula of the form $h = h_0 r^p$, where r is the distance to the closest major body in the integration and p is chosen empirically provides an acceptable compromise between speed and numerical accuracy. For orbits as elliptical as 109P/Swift–Tuttle, a value of $p = 1.5$ is close to optimum in the product of integration time and final total accumulated error, and we use this throughout. Other integration

TABLE I
Formula for Ejection Velocity for Each Model Variant

Model no.	Name	Ejection formula
1	Crifo distributed production	$\log_{10}(V_{\text{eject}}) = -2.143 - 0.605 \log_{10}(\text{radius}) - 0.5 \log_{10} r$ $P(V - V_{\text{eject}}) = \frac{1}{e^{3.7}} \exp\left[\frac{3.7 - 10.26(V - V_{\text{eject}}) + 4.12(V - V_{\text{eject}})^2}{1 - 1.03(V - V_{\text{eject}}) + 0.296(V - V - V_{\text{eject}})^2}\right]$
2	Jones ejection distribution with modified heliocentric velocity dependence	$V_{\text{eject}} = 10.2 r^{-0.5} \rho^{-1/3} R_c^{1/2} m^{-1/6}$ $P(V - V_{\text{eject}}) = 1$ for $V = V_{\text{eject}}$ and 0 otherwise
3	Jones ejection distribution	$V_{\text{eject}} = 10.2 r^{-1.038} \rho^{-1/3} R_c^{1/2} m^{-1/6}$ $P(V - V_{\text{eject}}) = 1$ for $V = V_{\text{eject}}$ and 0 otherwise
4	Jones ejection distribution with parabolic probability distribution	$V_{\text{eject}} = 10.2 r^{-1.038} \rho^{-1/3} R_c^{1/2} m^{-1/6}$ $P(V - V_{\text{eject}}) = 1 - \left(\frac{V}{V_{\text{eject}}} - 1\right)^2$ for $0 < V < 2V_{\text{eject}}$ and 0 outside

schemes are available which are superior in speed and produce somewhat more precise results. For our purposes, however, the RK4 integrator is entirely adequate and has been tested against output from SWIFT and RADAU and found to show no variations of significance within our range of adopted bin sizes in parameter space.

To further speed up integrations, the $(n - 1)^2$ computations normally found in n-body calculations (and general features of other solar system integrators) was removed entirely by generating predefined planetary position tables in memory. These tables were derived from the DE404 JPL planetary ephemeris and are stored in memory with planetary positions interpolated via cubic splines to accuracies (relative to the original DE404 ephemeris) no worse than 100 km for the positions of the major planets over the past 2000 years, with average errors nearly one order of magnitude better than this value.

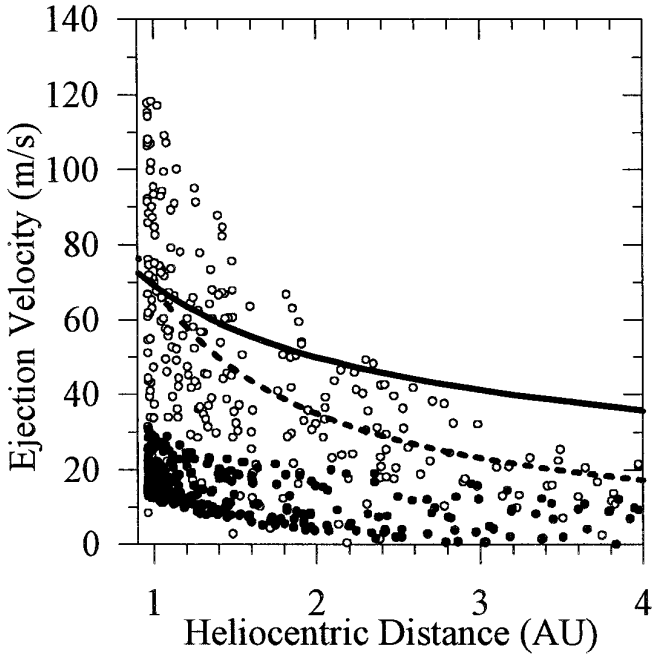

FIG. 1. Sample velocity ejection distributions for Perseids ejected in 1862 of mass 0.01 g and density 800 kg m^{-3} as a function of heliocentric ejection distance. Model 1 meteoroids are shown as filled circles, Model 2 as a solid line, Model 3 as a dotted line, and Model 4 meteoroids are shown as open circles.

All numerical computations are performed taking into account planetary perturbations, barycentric corrections, radiation pressure, and the Poynting–Robertson effect (cf. Burns *et al.* 1979) for a detailed description of the latter two forces). The barycentric corrections are significant for orbits as large and elliptical as 109P/Swift–Tuttle (cf. Chambers 1995) and necessitated an upper limit of between 0.2–0.4 years in the largest step size, independent of distance to the nearest perturbing body.

The above integrations required approximately 4 months of continuous computation on 5 Pentium PCs.

4. RESULTS

4.1. Previous Perihelion Passage (1862)

We begin by examining the meteoroid distribution at the present epoch due to Perseids ejected in 1862. Some general comments concerning the overall evolution of the modeled meteoroids from 1862 to the present are in order. It was found that Models 2 and 3 show virtually identical outcomes both in terms of flux as a function of time and solar longitude of maximum in any given year, locations of radiants, stream dispersion, etc. The choice of $r^{-0.5}$ or r^{-1} dependence on the ejection velocity was found to be the most insensitive variation among models from 1862 and always resulted in very similar final distributions. As the majority of the meteoroids are ejected near perihelion

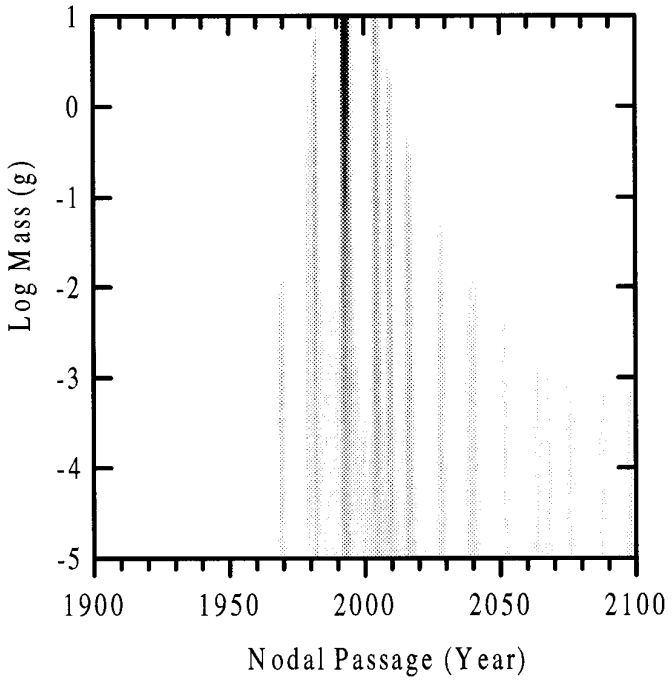

FIG. 2. Activity at the present epoch from ejecta released in 1862 for Model 32. The gridding is 1-year bins for the nodal passage time and 0.1 in log M. The grayscale has a dynamic range from 0 to 700 for this binning size.

(as required by the condition of random distribution in true anomaly) the small number of more distant ($r > 2$ AU) ejections does not make a strong contribution to the overall activity of the stream presently observed. The only noticeable difference between the more distantly ejected population ($2 < r < 4$ AU) and meteoroids ejected near perihelion is a larger spread in nodal longitudes for the former which becomes particularly evident at small masses.

Figure 2 shows a temporal plot of the distribution by mass of test meteoroids having nodes within 0.005 AU of the Earth's orbit from Model 32. We use 0.005 AU as our sieving distance and hereafter refer to all such meteoroids as Earth intersecting. There is an obvious periodicity in the figure apparent in all model variants of ejecta from 1862. Figure 3 shows a plot of nodal distance versus time for model 42 meteoroids of mass 10^{-2} g demonstrating that the reason for the periodicity is an impulsive change in the mean nodal distance of shower meteoroids inward every 12 and 30 years. This effect is the result of distant, direct perturbations on the stream by Jupiter and Saturn and is developed in more detail in Section 5.1.

In general, all models show that the most recent activity associated with the 1862 ejecta is concentrated from 1991 to 1994 with a peak in 1993. It is clear from Fig. 3 that meteoroids not perturbed by planetary perturbations after ejection in 1862 have nodes outside Earth's orbit, a result which holds for all models and all masses. In rare cases, smaller meteoroids (generally of higher density) ejected with high velocities can reach within 0.005 AU outside of Earth's orbit and be counted as possible "impacts" in years well away from the inward nodal shifts due to planetary perturbations, but this number is very small. Some activity is also apparent near 1980 and near 2010 at much lower levels.

For activity in any year from 1992 to 1994, the distribution of nodes for all models is strongly concentrated in the region from 139.3° to 139.6° (J2000) with maximum in the region 139.42°–139.5°. This result changes with cone angle in such a way that smaller cone angles tend to concentrate the peak into a smaller range of solar longitude centered about the node of the comet (139.44°) as would be expected. The particle distribution in these years from the 1862 ejection is also heavily skewed toward the largest (lowest ejection velocity–least radiation pressure affected) masses.

The model-determined radiant size (the rms dispersion in solid angle for the ensemble of all Perseid meteoroid geocentric radiants) is determined entirely by the distribution of initial ejection velocities and for the models used here, the 1862 radiant rms diameter is ~0.1°. The location of the radiant varies from year to year by a small amount

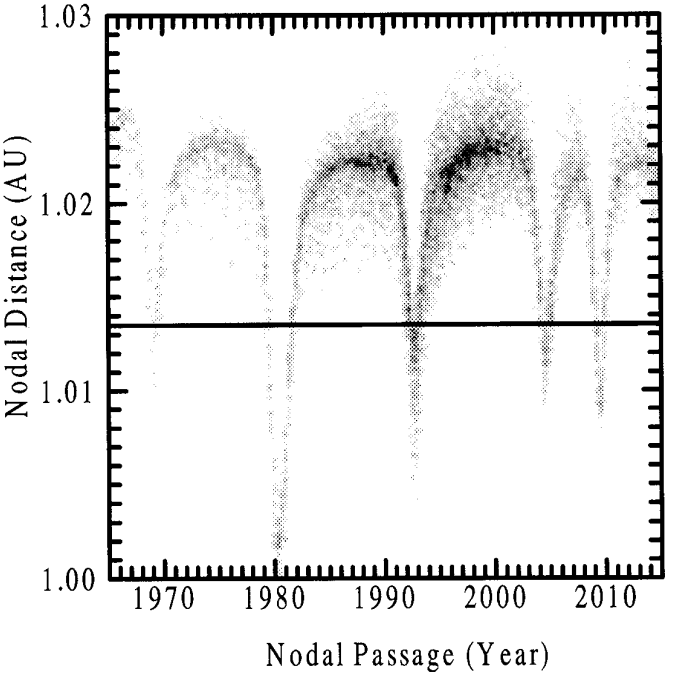

FIG. 3. Nodal distance versus time for meteoroids ejected in 1862 from Model 42 of mass of 0.01 g. The nodal points are gridded to a resolution of 0.0002 AU. The Earth's distance at the time of Perseid maximum is 1.01355 AU and is shown by the bold horizontal line. The grayscale has a dynamic range of 0 to 19 for this binning resolution.

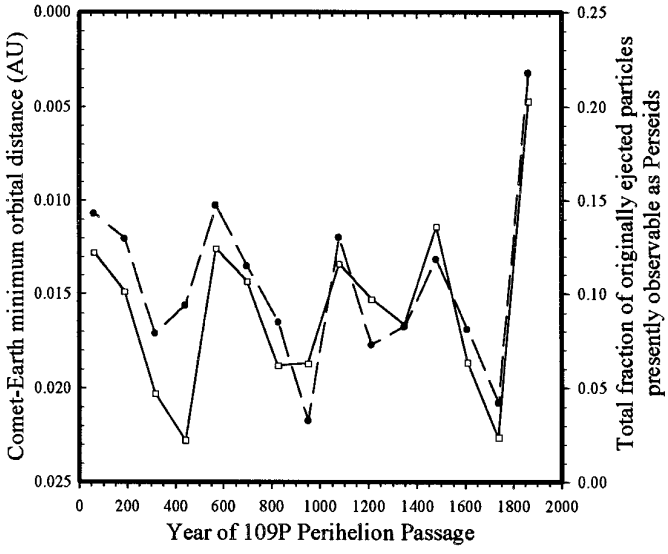

FIG. 4. The minimum comet–Earth distance for 109P/Swift–Tuttle (open squares) and the fraction of Perseid meteoroids from all models and all masses which currently are Earth-intersecting from each ejection interval (solid circles).

(about 0.3° in declination and 0.2° in RA) due to differential planetary perturbations (see Discussion).

4.2. Recent Ejections (2000 Years)

Results of ejections from 109P/Swift–Tuttle at each perihelion passage from 59 to 1610 AD were carried out at 7 discrete mass intervals separated by one order of magnitude in mass in the range $10–10^{-5}$ g. For completeness, the same mass categories were extracted from the more extensive runs from 1737 and 1862.

The final distributions of meteoroids at the present epoch reveal that the difference in closest approach between the comet and Earth at the epoch of ejection is a strong determinant of subsequent activity.

Figure 4 shows a plot of the minimum approach distance between the osculating orbit for 109P/Swift–Tuttle at the epoch of each perihelion passage (listed as years in the abscissa) and the Earth. The dashed line shows the total number of meteoroids from all models ejected from each passage which still have nodes within 0.005 AU of Earth at the nodal passage closest to the 1992 perihelion date. There is no significant correlation between the age of ejection over this time interval and the fraction of all ejected meteoroids currently in Earth-intersecting orbits. This finding suggests that the Earth–comet orbit distance at the time of ejection, rather than planetary perturbations, control the large-scale delivery of Perseid meteoroids on this time scale. It is for this reason that material ejected in 1737 and 1610, though quite young, is expected to be less prolific on average at present than ejecta from 1479. Indeed, it is found that for the years from 1995 to 1997, for example, the material from 1479 is the dominant Perseid population observed at the Earth for the outburst portion of the stream. A similar trend is seen for each model, further indicating that neither the assumed particle density nor the ejection velocity play a dominant role in the subsequent encounter conditions with Earth.

The total number of Earth-intersecting Perseids as a function of time at the present epoch summed over all ejecta for meteoroids capable of producing visual meteors ($>10^{-3}$ g) and larger over the past 2000 years is shown in Fig. 5 for three representative models. The general form of the activity is similar for all 12 model variants, namely, a 12- and 30-year periodicity reaching peak strength near 1992–1993. For each ejection model, higher meteoroid densities yield more Earth-intersecting meteoroids, a result of the general trend toward larger nodal distances as radiation pressure increases (see Section 5.1). The year of ejection-yielding meteoroids varies significantly from year to year in the current epoch; as a result, we expect that the position of peak activity in the stream for the outburst component will similarly vary.

The rms angular width of the radiant as a function of time is shown in Fig. 6. Here we have plotted the rms spread in the distribution of individual geocentric radiant points calculated from each Earth-intersecting visual-sized Perseid and added the distributions in a cumulative manner. Hence, the value at 2000 years is the angular spread in the total radiant area from all 15 perihelion ejections from 59–1862 AD. Note that the positions of the radiants from any one ejection vary in RA and DEC due to planetary perturbations; thus, the rms spread in this cumulative radiant size plot is greater than the rms radiant sizes found from individual ejections. The initial size of the radiants and early evolution of the size of the radiant area are controled by the ejection velocity, with higher average velocities having larger initial dispersions, but within 500 years (roughly 4 passages) the absolute levels of spread vary inversely with the density of the meteoroids for all models. This suggests that in the longer term, the absolute level of rms spread is controled by radiation pressure primarily and to a lesser degree by the initial ejection velocity. However, the slope of the radiant dispersion is constant and similar for all models, showing that planetary perturbations and initial ejection comet–Earth geometry are the ''drivers'' of radiant shape.

A regression fit to the radiant spread from 500 to 2000 years yields an annual change of 6.5×10^{-5} degrees/annum. The particularly small values for Model 1 are a direct consequence of the extremely low ejection velocities of the extended source production model. The correctness of the above conclusions can be gauged on the basis of the very low initial dispersion for Model 11 due to the extremely low ejection velocities for larger particles in Model

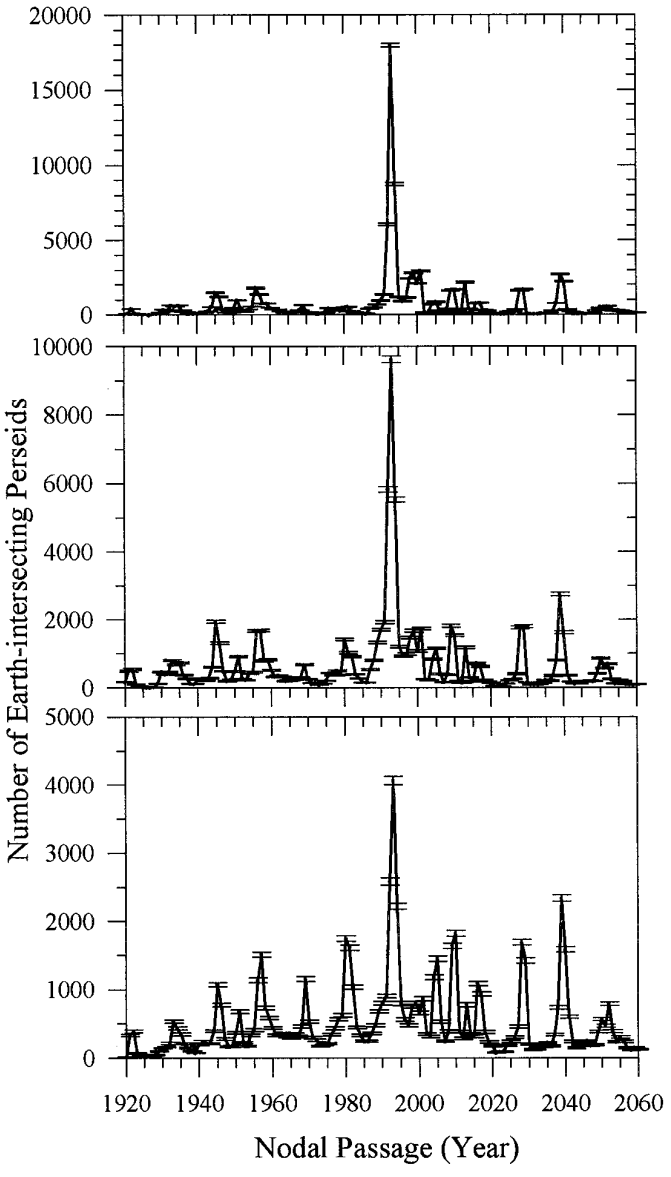

FIG. 5. The number of Earth-intersecting Perseids versus their nodal passage time in total for all ejections from 59–1862 AD for Models 12 (top), 33 (middle), and 41 (bottom). Activity is summed into yearly bins and the error bars represent the poisson error margins ($n^{-1/2}$).

11 (or equivalently for lower density particles of the same mass—the opposite to the dependence from the other models—see Eq. (6)) and its sudden relative increase to Models 12 and 13 after 4–5 revolutions as the full effects of radiation pressure expand the radiant.

The scatter in the rms spread at any one time between all models is on the order of 0.1° over this 2000-year period. The location of the radiant after the full 2000 years of accumulated ejections (i.e., now) over the mass range 0.1–10 g (photographic) is $\alpha = 46.09 \pm 0.02$ and $\delta = 57.66 \pm 0.02$ (J2000.0). The variation in α throughout this time is very linear and well represented by $\alpha = 45.88 + 1.128145 \times 10^{-4}\ Y$, where Y is the year of the last included ejection figured backward in time in the summation referenced to an origin at 2000 AD. The declination shows much more scatter during the past 2000 years as it depends more on planetary perturbations than α (which is more closely linked to the progression of the node). The variation is approximately represented by $\delta = 57.67 + 10^{-5}\ Y$. All radiant measures are referenced to J2000 and $\lambda_0 = 139.7°$ (139.0° B1950.0).

The locations and strength of the observed visual peak associated with the outburst component of the stream derived from Brown and Rendtel (1996) and from Rendtel and Arlt (1996) are shown in Fig. 7, together with the model predictions for the same quantities. The locations of the visual peaks in outburst activity and their shape were found by taking the average Perseid zenithal hourly rate (ZHR) profile from Brown and Rendtel (1996) over the period 1988–1994 and subtracting this profile from each years' activity after scaling for differences in peak activity between the average profile and each yearly profiles' main (or normal) maximum ZHR value. Note that the visual observations refer to Perseid meteoroids with masses of 10^{-4} g and larger, with the average mass near 1 mg (corresponding to a visual absolute magnitude of +3 at Perseid velocities). It was found that the mean curve of Perseid ZHR activity from 1988 to 1994 in the interval from $139° < \lambda_0 < 140.1°$ is well approximated by

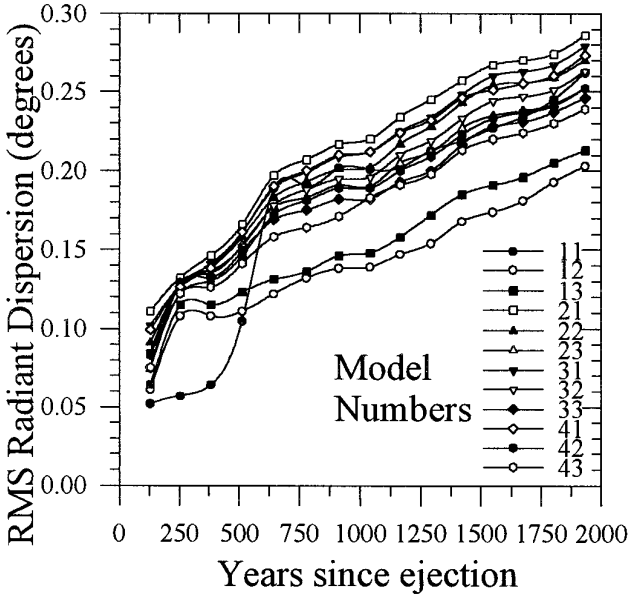

FIG. 6. Root-mean squared (rms) spread in radiant size for all models as cumulative distributions observed at present from ejections between 59 and 1862 AD. The time in years (abscissa) refers to years before present (i.e., year 0 is 2000 AD).

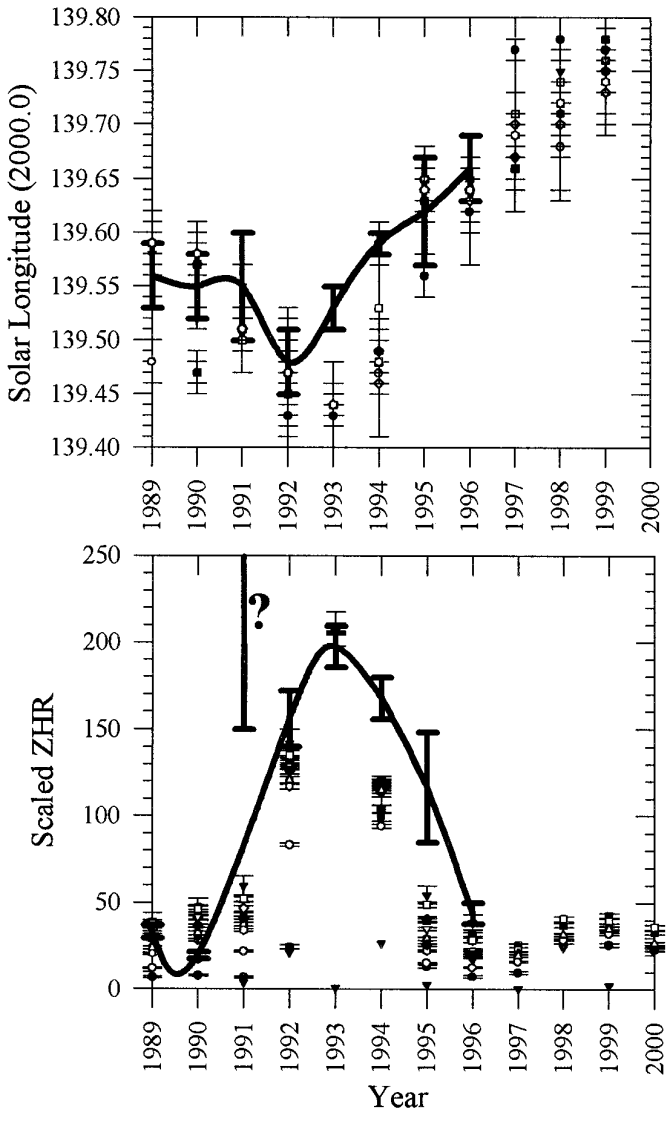

FIG. 7. Locations (J2000) of outburst peak for the Perseids (bold solid line) together with model predictions of peak locations (top). The scaled ZHR for the observed outburst peaks from 1989 to 1996 and individual model predictions are also given (bottom). Symbols for each model variant for both graphs are the same as given in Fig. 6. Observational data are from Brown and Rendtel (1996). The question mark next to the 1991 observation reflects the high uncertainty in this value (see Brown and Rendtel (1996)). The solid curve is formed without using the 1991 value.

$$\mathrm{ZHR} = 1.84110984 \times 10^8 - 3.95803796 \times 10^6 \lambda_0 + 28363 \lambda_0^2 - 67.67 \lambda_0^3. \quad (8)$$

It is clear from Fig. 7 that the predicted and model times of peak are generally in good agreement, with the exceptions of the 1993 and 1994 peak locations, where model values are 1–2 h earlier than observed. The overall trend of observed changes in peak location and the model locations are consistent, reflecting the dominance of older ejecta before 1992 and after 1994 (see Table II). Note that the ZHR of the outburst peak in 1988 was found to be of negligible magnitude after subtraction of the mean scaled background, drawing into doubt the reality of the feature in 1988 and we omit it from further analysis. The move in the time of the peak away from the current nodal longitude (139.44°) of Swift–Tuttle reflects the fact that 109P's nodal longitude has been higher than its present value for most passages over the past 1000 years (contrary to its long-term behavior) and hence slightly older ejecta are now well ahead of the comet's nodal longitude. This ejection geometry implies that ejecta from as recently as 1348 can be found as late at nearly 139.8° at the present epoch, all other ejections over the past 2000 years peaking earlier. The cumulative activity for visual-sized meteoroids is shown in Fig. 8 for two representative models as a function of solar longitude. All meteoroids ejected over the past 2000 years currently have nodal longitudes greater than 139° and the profile from just these 15 ejections already shows remarkable similarity to the shape of the "core" Perseid activity found from visual observations, the asymmetry of both being particularly notable.

The relative change in the strength of the peaks is reproduced, though the peak observed ZHR in 1991 (which has large error margins) does not fit the trend well, the model underestimates its strength. A similar, though less substantial effect, is also seen in 1994 and 1995, suggesting that for the strongest years the model tends to underestimate peak ZHR activity.

Table II summarizes the composition of the Perseid activity (all of the outburst peak and part of the core activity of the stream) in terms of the summation of all ejections (59–2000 AD) for each of the years from 1988 to 1996 for visual class meteoroids. The total number of Earth-intersecting test meteoroids as well as the fraction of this total contributed by the three most significant ejections are also shown. It can be seen that the activity for all models peaks in 1992–1993 and that the makeup of the ejecta observed as the outburst component of the Perseids changes dramatically from year to year. In 1988–1990, ejections from 1610 and 1737 are predominant and account for the majority of the activity, while in 1991 material from 1862 and 1610 is found in roughly equal proportions. The 1991–1994 outburst maxima are composed primarily of material from 1862 and to a lesser degree 1610. Note that even in these years, the fraction of all meteoroids of recent origin (the past 2000 years) is still greater from all earlier passages than from 1862 alone. In 1995 and 1996 the origin of the outburst material changes again, with 1479 dominant and 1079 and 1862 making contributions.

The model peaks generally follow closely to one another. A glaring exception here is Model 11, which shows marked

TABLE II
Number of Earth-Intersecting Perseids by Year (1988–1996) and Model at the Present Epoch

	11	12	13	21	22	23	31	32	33	41	42	43
1988	95	472	748	589	688	716	471	655	800	474	626	724
	441 0.24	1737 0.71	1737 0.56	1610 0.26	1610 0.39	1610 0.48	1610 0.36	1610 0.41	1610 0.42	1610 0.31	1610 0.38	1737 0.46
	698 0.24	1610 0.15	1610 0.32	1862 0.16	1737 0.20	1737 0.31	1737 0.23	1737 0.34	1737 0.42	1737 0.26	1737 0.37	1610 0.37
	59 0.13	441 0.04	826 0.03	1479 0.15	1479 0.10	826 0.05	826 0.08	826 0.05	826 0.04	1862 0.10	826 0.04	826 0.04
1989	122(1.73)	691(1.14)	1178(.93)	659(.45)	961(.31)	1277(.27)	678(.14)	948(.45)	1327(.39)	680(.42)	871(.37)	1171(.47)
	698 0.21	1737 0.52	1610 0.49	1610 0.32	1610 0.49	1610 0.55	1610 0.44	1610 0.52	1610 0.57	1610 0.40	1610 0.52	1610 0.55
	188 0.19	1610 0.37	1737 0.40	1862 0.17	1737 0.18	1737 0.22	1737 0.17	1737 0.24	1737 0.29	1737 0.19	1737 0.28	1737 0.31
	59 0.17	59 0.04	59 0.03	1479 0.15	1479 0.12	1479 0.08	1479 0.11	1479 0.08	1479 0.04	1479 0.09	1479 0.07	1479 0.04
1990	144(.36)	965(.97)	1681(.95)	827(.46)	1168(.51)	1585(.79)	831(.48)	1272(.57)	1696(.81)	802(.70)	1185(.72)	1628(.88)
	1348 0.31	1610 0.48	1610 0.54	1610 0.39	1610 0.50	1610 0.58	1610 0.47	1610 0.54	1610 0.60	1610 0.43	1610 0.54	1610 0.58
	698 0.14	1737 0.45	1737 0.37	1862 0.20	1737 0.18	1737 0.23	1737 0.18	1737 0.22	1737 0.29	1737 0.19	1737 0.25	1737 0.31
	188 0.14	59 0.02	1479 0.03	1737 0.10	1479 0.10	1479 0.07	1862 0.08	1479 0.09	1479 0.06	1862 0.11	1479 0.07	1479 0.05
1991	124(1.51)	1351(.97)	2127(.88)	927(.76)	1282(.54)	1689(.66)	940(.41)	1308(.77)	1916(.77)	909(.47)	1372(.68)	1955(.89)
	59 0.20	1862 0.37	1610 0.38	1862 0.31	1610 0.34	1610 0.39	1862 0.35	1862 0.36	1862 0.39	1862 0.36	1862 0.37	1862 0.39
	569 0.20	1610 0.36	1862 0.36	1610 0.25	1862 0.33	1862 0.33	1610 0.29	1610 0.34	1610 0.35	1610 0.28	1610 0.33	1610 0.35
	698 0.11	1737 0.23	1737 0.20	1737 0.10	1737 0.12	1737 0.14	1737 0.11	1737 0.15	1737 0.17	1737 0.11	1737 0.16	1737 0.18
1992	448(.82)	6071(.24)	8063(.2)	2100(.75)	3240(.56)	4586(.31)	2428(.51)	3926(.32)	5827(.22)	2588(.32)	4410(.18)	6692(.21)
	1862 0.44	1862 0.47	1862 0.43	1862 0.29	1862 0.37	1862 0.41	1862 0.37	1862 0.40	1862 0.43	1862 0.38	1862 0.43	1862 0.44
	826 0.18	1610 0.15	1610 0.19	1610 0.15	1610 0.15	1610 0.16	1610 0.12	1610 0.14	1610 0.15	1610 0.13	1610 0.14	1610 0.16
	1079 0.11	1737 0.07	1479 0.08	1479 0.10	1479 0.10	1479 0.08	1479 0.09	1479 0.09	1737 0.09	1479 0.08	1737 0.08	1737 0.09
1993	3780(4.96)	17971(4.16)	20120(3.86)	2971(5.56)	5142(3.61)	7714(3.94)	3741(5.46)	6334(3.93)	9623(3.89)	4064(3.88)	7586(3.97)	11896(3.75)
	1862 0.70	1862 0.49	1862 0.42	1862 0.32	1862 0.37	1862 0.39	1862 0.38	1862 0.38	1862 0.39	1862 0.37	1862 0.39	1862 0.40
	826 0.04	1610 0.12	1610 0.15	1610 0.17	1610 0.16	1610 0.19	1610 0.14	1610 0.16	1610 0.17	1610 0.14	1610 0.16	1610 0.15
	1079 0.03	1079 0.06	1079 0.07	1079 0.09	1079 0.09	1079 0.11	1079 0.09	1079 0.10	1079 0.10	1079 0.09	1079 0.10	1079 0.09
1994	1804(2.86)	8773(4.01)	9094(5.06)	1542(3.54)	2578(4.48)	4213(5.24)	2112(5.44)	3693(4.82)	5539(4.68)	2222(5.24)	4196(5.45)	6661(5.21)
	1079 0.18	1079 0.18	1862 0.21	1862 0.34	1862 0.34	1862 0.28	1862 0.36	1862 0.35	1862 0.32	1862 0.31	1862 0.34	1862 0.32
	569 0.16	1862 0.15	1079 0.12	1479 0.19	1479 0.15	1610 0.16	1610 0.17	1610 0.18	1610 0.16	1479 0.12	1610 0.14	1610 0.12
	826 0.16	826 0.14	826 0.12	1079 0.09	1610 0.10	1479 0.14	1479 0.10	1479 0.09	1079 0.12	1610 0.12	1079 0.10	1079 0.12
1995	241(0.38)	1189(0.16)	1482(0.04)	779(0.05)	983(0.30)	1183(0.22)	881(0.23)	1071(0.23)	1199(0.16)	795(0.25)	1072(0.03)	1283(1.23)
	1079 0.29	1479 0.32	1479 0.49	1479 0.40	1479 0.49	1479 0.56	1479 0.36	1479 0.46	1479 0.59	1479 0.41	1479 0.50	1479 0.55
	569 0.14	1079 0.24	1079 0.15	1862 0.27	1862 0.19	1079 0.12	1862 0.27	1862 0.15	1079 0.12	1862 0.20	1862 0.12	1079 0.14
	950 0.14	569 0.10	698 0.09	1079 0.07	1079 0.09	1862 0.08	1079 0.07	1079 0.07	950 0.05	1079 0.06	1079 0.09	826 0.07
1996	132(3.51)	926(1.35)	1231(1.19)	592(0.82)	795(1.20)	934(0.90)	513(1.71)	698(1.20)	921(0.87)	559(1.50)	791(0.94)	1072(5.54)
	1079 0.20	1479 0.44	1479 0.53	1479 0.48	1479 0.65	1479 0.69	1479 0.50	1479 0.66	1479 0.71	1479 0.51	1479 0.62	1479 0.66
	569 0.19	1079 0.20	1079 0.13	1862 0.24	1862 0.10	1079 0.09	1862 0.14	1079 0.06	1079 0.08	1862 0.14	1079 0.08	1079 0.10
	950 0.14	569 0.09	698 0.08	1079 0.05	1079 0.05	698 0.04	1079 0.09	1862 0.06	826 0.04	1079 0.08	826 0.06	826 0.06
Totals	6890 (16.13)	38409 (13.0)	45724 (13.11)	10986 (12.39)	16837 (11.51)	23897 (12.33)	12595 (14.38)	19905 (12.29)	28848 (11.79)	13093 (12.78)	22109 (12.34)	33082 (18.18)

Note. Numbers in parentheses give the rms variance in the fit between each model and the observed ZHR distributions. The total number of visual-sized Perseids encountered by Earth ($m > 0.001$ g) is also given on the same line. The three main contributing ejection epochs and fraction of all Perseids recorded in a particular year due to these three main contributing ejection epochs are also listed.

deviation from the other models and the observed peak locations. This anomaly may be explained in part by the relatively small number of meteoroids from this model in several of the examined years. As well, the ejection conditions for this model (low-density meteoroids, with low-ejection velocities) may be unrealistic. The distribution of variances of fit between the predicted times of maximum and the observed are quite small for all models (except Model 11), with the best overall fit being due to Model 21. Indeed, Model 21 is the only model which agrees with the observed times of peak within error for all 8 years, except 1993.

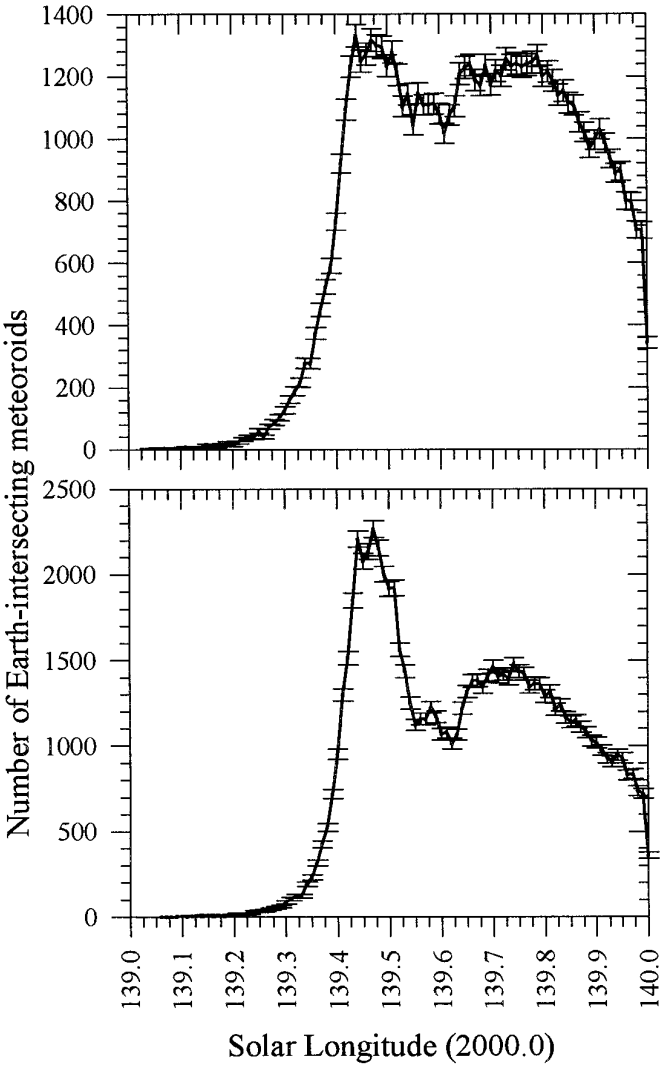

FIG. 8. Cumulative activity as a function of solar longitude for Models 22 (top) and 33 (bottom) from the past 2000 years of ejections from Swift–Tuttle.

The coefficient of relative fit for each year and for each model is also given in Table II in parentheses after the total number of test meteoroids encountered in a given year. This value is found from the subtraction of the observed outburst profile for each year with the normalized number of test meteoroids found in every equivalent solar longitude bin (to a resolution of 0.01°) from 139°–140° and the summation of the squares of the difference between the observed and theoretical profile in this interval. Note that the difference in fit between years is not significant in general, owing to differing numbers of observational intervals from year to year with only intermodel comparisons having meaning for one particular year.

The totals in the last row suggest that the ZHR profiles in these years can best be represented by Model 22 (Jones ejection velocity with $r^{-0.5}$ heliocentric velocity dependence), though the difference between many models is not large. The exceptions here are Models 43 and 11, which have unusually large variances in fit between the observed and theoretical profiles.

4.3. Long-Term Evolution (100,000 Years)

To study the behavior of the Perseids over a significant fraction of the lifetime of the stream (variously estimated to be as much as 250,000 years of age (cf. Hughes 1995)), one must first know the orbit of the comet. Unfortunately, one cannot, as 109P/Swift–Tuttle has been observed only since 69 BC (Yau *et al.* 1994). The chaotic effects of random errors in initial conditions imply that the position and ultimately the orbital elements of the comet quickly diverge during backward integrations.

Chambers (1995) investigated the long-term motion of Swift–Tuttle both forward and backward. He found that the comet's past behavior implied a Lyapunov exponent of approximately 180 years in the immediate past, and he found the comet's current and future motion to be influenced by the 1 : 11 libration Swift–Tuttle currently experiences with Jupiter.

To attempt to model the stream, we need plausible past orbital elements for the comet and find these by taking the six-vector of the comet (velocity vector and position vector) at perihelion in 1862 and ''cloning'' 20 different seed orbits about the nominal position of the comet within a sphere of radius 10 km (comparable to the size of the nucleus of the comet). Each seed orbit was then integrated backward in time using the SWIFT symplectic integrator (cf. Levison and Duncan 1994) with a time step of 0.25 days for 100,000 years using the JPL DE404 ephemeris to generate all initial planetary positions and velocities. Of greatest importance to the visibility of the Perseid stream on Earth at the present time is the distance of the descending node of the comet from Earth's orbit. This is shown at 300-year increments for all 20 cloned orbits for the full integration time in Fig. 9. The general position of the node over this time is remarkably close to the Earth, a result also found by Chambers (1995). Indeed, for the past 20,000 years, no nodes are found outside $0.9 < R_d < 1.15$, a remarkably similar finding to Chambers (1995). From the ensemble of cloned orbits, two orbits were chosen at intervals of approximately 5000, 10,000, 20,000, 50,000, 75,000, and 100,000 years. The two orbits were selected to be the most ''extreme'' from the set in the sense of having the largest or smallest semimajor axis. The orbital elements used for each of these two seed orbits (1 for the lower values and 2 for the larger values of a) are given in Table III. Using these input orbits, a full set of test Perseid starting orbits was generated using a Model 42 variant (which was felt at the outset to be most representative) for ejection

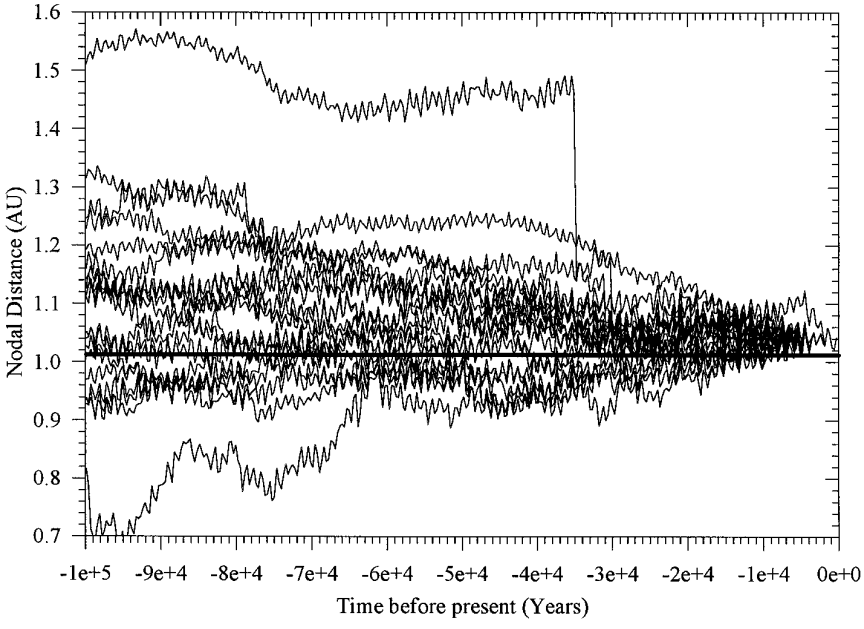

FIG. 9. Nodal distance of 20 cloned variations of 109P/Swift–Tuttle over the past 100,000 years shown at 300-year intervals.

velocities as with the shorter term integrations. By comparing the final results of these simulation runs, we hope that some indication of the importance of the cometary starting orbit can be inferred and thus the probable error in the simulation, given that the true orbit this long ago is not a posteriori known.

The final distributions of meteoroids at the present time show much less temporal variation than did the test particles from integrations over the past 2000 years as might be expected. Even ejections only 5000 years of age show a surprisingly constant annual level of activity with an average of roughly 30 Earth-intersecting meteoroids encountered per year. Some small periodic variations in the annual influx from orbit 1 for ejection 5000 years ago is evident—possibly attributable to the accumulated effects of jovian impulses (see Section 5.1). The number of Earth-intersecting test meteoroids drops off nearly linearly in time for orbit 2, but much slower for orbit 1 particles. This effect is attributable to the node of orbit 1 being inside the Earth's for more recent cometary starting orbits re-

TABLE III
Initial Seed Orbits (1 and 2) for Perseid Integrations from 100,000 Years to the Present at the Intervals Shown in the First Column

Ejection	a	e	i	ω	Ω	T
5000	25.21880	0.9605500	114.755	151.850	137.475	−6990.0
	28.14470	0.9656100	113.121	152.250	138.321	−6990.0
10000	24.59700	0.9617600	114.866	152.909	136.251	−11989.0
	30.34540	0.9685600	112.882	153.146	136.833	−11989.0
20000	22.97440	0.9567600	116.881	150.168	132.322	−21990.0
	31.78580	0.9691800	113.291	156.677	133.632	−21990.0
50000	22.06170	0.9574700	118.929	156.287	114.114	−51990.0
	37.59280	0.9714600	111.332	154.537	128.582	−51990.0
75000	21.40130	0.9495200	123.386	150.150	108.858	−76990.0
	39.68530	0.9728500	111.641	156.933	124.972	−76990.0
100000	20.72780	0.9357000	120.977	175.776	83.694	−101980.0
	49.09810	0.9808400	113.213	163.645	119.646	−101980.0

Note. Other columns list the osculating orbital elements at T, the epoch of perihelion, given in units of years before January 1, 2000.

TABLE IV
Locations and Widths of the Maximum for Each Ejection for Earth-Intersecting Perseid Meteoroids at the Present Epoch

Time since ejection	λ_{peak}	Width
6990.0	140.56° ± 0.02°	1.70° ± 0.02°
	140.85° ± 0.03°	1.90° ± 0.03°
11989.0	140.04° ± 0.04°	1.67° ± 0.04°
	139.81° ± 0.08°	2.46° ± 0.08°
21990.0	141.55° ± 0.09°	2.30° ± 0.1°
	139.62° ± 0.14°	2.80° ± 0.16°
51990.0	133.31° ± 0.11°	4.59° ± 0.11°
	140.13° ± 0.32°	7.36° ± 0.32°
76990.0	146.99° ± 0.26°	8.00° ± 0.26°
	139.39° ± 0.42°	8.95° ± 0.42°
101980.0	122.99° ± 0.86°	15.31° ± 0.95°
	136.00° ± 0.78°	11.07° ± 0.78°

sulting in easier delivery of meteoroids to Earth as radiation pressure preferentially moves the nodes (on average) further outward (see Section 5.1).

The distribution in solar longitude of meteoroids for older ejections is given in Table IV. The locations of the maximum for long-term ejecta at the present epoch, found by fitting a Gaussian to the present distribution of modeled meteoroid nodal longitudes, shows a slight decrease in position with age, the maximum position following $\lambda_0 = (141.05 \pm 0.08) - (3.23 \pm 1.23) \times 10^{-5}\ Y$. This relation would imply that the rate of nodal progression is very similar for all ejecta and the parent comet up to 5000 years ago. This relation also explains the asymmetry in the broad rate profile of the shower, namely that past ejections ''pile up'' in the region 139–141 with the older ejections occurring predominantly in the earlier portions of this interval. Note that this relation does not take into account the position of current ejecta maximum (more recent than ~6000 years ago) located closer to the comet's current nodal longitude than these much older ejecta and which peak roughly 1.5° earlier than the above relation would suggest.

The Gaussian half-width of the nodal distribution profiles of Earth-intersecting meteoroids at the present epoch (in degrees) follows the relation

$$W = (0.774 \pm 0.550) + (9.183 \pm 0.830) \times 10^{-5}\ Y. \quad (9)$$

This demonstrates how the stream can be so long-lived at the current epoch given even a modestly long age (see Section 5.4), with ejections 100,000 years ago currently having full widths of nearly 25° in solar longitude.

The development of the stream over the past 100,000 years is summarized in Fig. 10, where nodal positions of test meteoroids at the present epoch are presented. The central portion of the meteoroid nodal footprint of the stream always remains very close to Earth for both orbits and all masses. The nodal distribution formed from orbit 2 shows considerably more elongation than orbit 1, reflecting the higher eccentricity and semimajor axis of the latter orbit and the large number of test meteoroids which move into sungrazing and near-sungrazing orbits (see Section 5.6).

5. DISCUSSION

The above results suggest the models used are not unreasonable representations of the actual ejection process of 109P/Swift–Tuttle, which is probably more complicated than our very simplified ejection schemes. In general, the two most reliably measured stream parameters, namely the activity as a function of solar longitude for each year and variations in peak activity from year to year as well as geocentric radiant distributions of shower meteors are consistent with the modeling results within the limitations of both (see Section 5.2 for a detailed comparison of the geocentric radiant distributions).

The investigation of the change in the final distribution of Perseid activity seen from Earth with variations in cone angle has revealed simply that the narrower cone angles tend to concentrate the resulting meteoroids more closely to the original comet nodal locations for recent ejections. Over periods on the order of 5 revolutions, the effects of narrower cone angles become masked as planetary perturbations begin to dominate the dispersion of the stream.

The one major discrepancy between the modeled results and observations which remains is the 1–2 h difference in peak time for the 1993 and 1994 Perseid outburst maxima, whose times of peak are known to better than 0.5 h. There are two possible explanations for the differences. One explanation could be that material associated with the outburst in 1993 and 1994 is richer in older ejections, implying that the comet was particularly active in 1610 or 1479, the two passages other than 1862 which our simulations suggest should contribute significantly to the outburst portion of the stream in these years. The ejecta from both of these passages would place the nodal longitude of the peak roughly 0.1° later than what is currently given by the models and could explain the discrepancy. The geometry of the comet's passage in 1610 and 1479 placed it well below the likely detection threshold for visual observations (Yau *et al.* 1994), and the fact that no observations exist for either of these returns suggests that the comet was not much intrinsically brighter than its long-term average. Alternatively, the ejection geometry in 1862 might have been much more collimated than the broader, hemispherical ejection geometry we have adopted. In particular, for ejec-

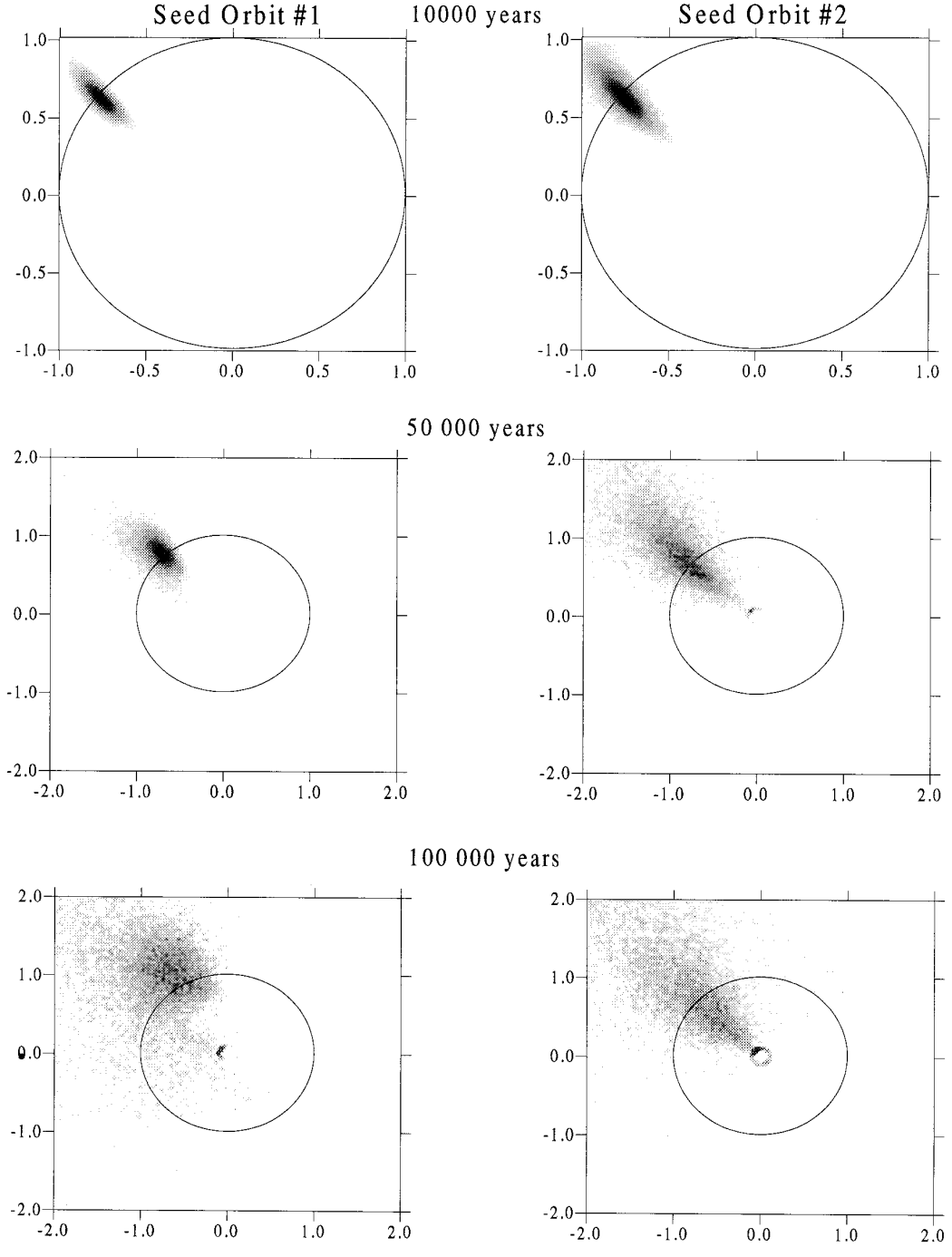

FIG. 10. Nodal distribution of all Perseid meteoroids of mass 0.1 g with ages shown at the present epoch for both initial seed orbits. The circular outline is the orbit of the Earth and all axis measurements are in AU.

tions with a substantial velocity component normal to the cometary plane, it is possible to change the mean nodal longitude as much as 0.1–0.2° with normal Whipple-type ejection velocities. More precisely, the change in nodal longitude can be described by (Roy 1978)

$$\Delta\Omega = \frac{r\sin(\theta+\omega)}{va^2\sqrt{1-e^2}\sin i}\Delta V_p, \tag{10}$$

where v is the mean angular velocity $(2\pi/T)$, θ is the true anomaly, and ΔV_p is the component of the velocity normal

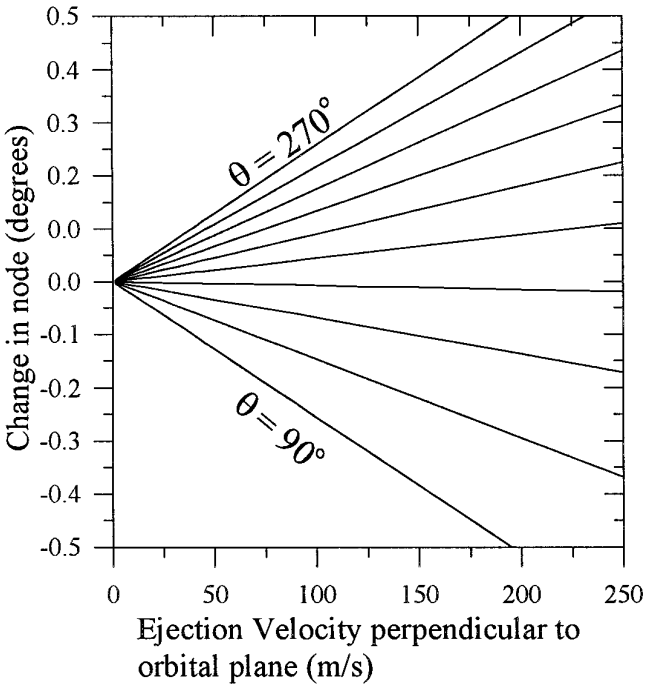

FIG. 11. Changes in the osculating nodal longitude at ejection of meteoroid test orbits as a function of the normal component (relative to the cometary orbital plane) of the initial ejection velocity and true anomaly (θ) at ejection. Each line represents values for the true anomaly from 270°–90° in steps of 20°.

to the orbital plane such that the object is seen to orbit in the counterclockwise direction as seen from this pole. Thus, to increase the nodal longitude from the initial ejection velocity alone requires a positive value for ΔV_p. Fortunately, detailed observations from the 1862 passage of Swift–Tuttle exist and these have been examined in detail by Sekanina (1981). In particular, he reconstructed the velocity vectors of the major jets near perihelion. Over the two-month period nearest perihelion, it was found that some 70% of all observed ejections had a velocity component with positive ΔV_p. Figure 11 shows the change in the osculating node as a function of the normal component of the ejection velocity and the ejection position along the orbit. For ejection preperihelion at a modest distance from the Sun ($r > 1.5$ AU) a velocity of less than 50 m/s is needed in the normal direction to produce a positive shift of 0.1° in the nodal longitude. This is well within the allowable range of ejection velocities for visual-sized meteoroids using the normal Jones/Whipple ejection model and suggests that the activity from 1993 and 1994 might best be explained by preperihelion ejection from isolated sites residing at latitudes significantly different from the subsolar point. Indeed, Sekanina (1981) noted that "...the net momenta exerted on the nucleus by ejecta from the active areas in 1862 were virtually all directed to the south of the orbital plane," implying that almost all ejections had a strong northward (positive V_p) component.

Perseid photographic data, representing roughly 600 orbits according to Lindblad and Porubcan (1994), also contains detailed distributions of all orbital elements. However, the previous discussion concerning large errors in the semimajor axis, for example, apply to lesser degrees to the errors for many other orbital elements and renders their usefulness questionable. The original data sources from whence these orbits are extracted often do not list estimates of the errors in other elements for individual orbits. An examination of the dispersion in mean elements from the simulation output yields standard deviations less than 0.003 AU in q, 0.5° in inclination, and 0.6° in the argument of perihelion for the combined ejections over the past 2000 years. For comparison, Spurny (1995) lists detailed data (and errors) for 27 Perseids photographed with fisheye cameras during the 1993 Perseids. His distributions show average errors of 0.005 AU in q, 1.1° in inclination, and 2.4° in the argument of perihelion. In all cases the average errors are 2 to 4 times the maximum dispersion in the cumulative theoretical distributions for the same elements. Porubcan (1977) examined most of the presently available Perseid orbits and showed that there is significant intersurvey differences in dispersion between the various photographic surveys. He concluded that the observed dispersions are greater than the true dispersion in the stream, a conclusion we also have reached. Of the several hundred Perseid orbits available, there is a small number of very precise orbits with errors smaller than our expected dispersions; in this case, however, the number of useable orbits drops to 1–2 dozen and thus no statistically meaningful comparisons can be made. We do not treat photographic orbital elements further and discuss only geocentric radiant distributions in the remainder of this work.

The considerable evolution experienced by some Perseid particles, particularly the changes in the argument of perihelion over time periods on the order of 50,000 years, resulted in movement of the ascending node of some test meteoroids to Earth intersection. The result was a shower of duration 2–3 weeks, which occurs in mid-March from the southern hemisphere. Table V provides orbital details of this theoretical twin shower of the Perseids, along with drift of the radiant point and spread in the radiant. A search for showers which might be associated with this theoretical radiant yielded two with close similarities—the Gamma Normids and the Theta Centarids (Jenniskens 1994). Both have radiant positions very close to our expected location and peak at very nearly the same nodal longitudes expected for the Perseid southern shower. The lack of velocity information for these streams means that the values for a, e, and q are uncertain—within these uncertainties the showers might be linked to the southern Perseid radiant. The Theta Centarids, in particular, show similarity

TABLE V
Orbital Elements and Radiant Location and Daily Drift for the Theoretical Perseid Southern Twin and the Same for Two Showers with Comparable Elements and Radiant Locations in Mid-March Taken from Jenniskens (1994)

Stream	a	e	i	ω	Ω	q	α	δ	$\Delta\alpha$	$\Delta\delta$
Theoretical Southern Perseid Twin	21 ± 3	0.99 ± 0.01	121 ± 21	76 ± 24	165 ± 22	0.61 ± .19	220	−43	0.99	−0.227
γ Normids	∞	1.0	133	41	172	0.89	249	−51	1.3	−0.2
θ Centarids	∞	1.0	128	27	153	0.90	210	−41	1.1	−0.4

to the theoretical stream and it would be most interesting to get accurate velocity information for these streams to test for any association.

5.1. *Planetary Impulses on the Perseid Stream*

Jupiter and Saturn pass within 1.6 and 0.9 AU of the orbit of 109P/Swift–Tuttle. The comet's high inclination is usually invoked to suggest direct planetary perturbations on the stream to be minimal and the stream quite stable. In broad terms this is certainly true as most stream meteoroids have moved in essentially the same general orbit as Swift–Tuttle for many thousands of years, a result confirmed by our direct integrations and others (cf. Hamid 1951).

However, as the Perseid stream is a continuous ring of meteoroids, some meteoroids always experience the maximum direct perturbations from either Jupiter or Saturn. Since at the present epoch the descending node of the parent comet is only very slightly outside Earth's orbit (0.004 AU outside for the 1862 passage), even small perturbations can move Perseid meteoroids from nonintersecting to Earth-crossing orbits.

In general, a Perseid meteoroid passing some distance from a planet will experience an impulse that changes its orbit by a small amount. This small perturbation results in a significant change in a and e since the orbit of 109P is quite eccentric. As the stream orbit does not pass close to any of the outermost planets (minimum distances from Uranus and Neptune are 2 and 6.5 AU, respectively), only Saturn and Jupiter are important in this regard. Figure 12 plots the envelope of closest possible distances between Jupiter and Saturn and the mean orbit of Swift–Tuttle. Any actual encounter between a Perseid meteoroid and one of these planets will have a planet–meteoroid distance curve inside these envelopes and with larger curvature. A typical encounter between Jupiter and a Perseid meteoroid is also shown in Fig. 12 (thin line).

For Earth-encounter, the heliocentric distance of the descending node must equal the Earth's orbital distance from the Sun. In general, the descending nodal radius in AU (R_d) is given by

$$R_d = \frac{a(1-e^2)}{1-e\cos\omega}, \tag{11}$$

where ω is the argument of perihelion. The change in the nodal radius due to variations in the individual osculating elements is given by

$$dR_d = R_d\frac{da}{a} + \frac{e}{1-e\cos\omega}[a(1-2e) + R_d\cos\omega]\frac{de}{e} + \frac{R_d e\sin\omega\, d\omega}{1-e\cos\omega}. \tag{12}$$

Typically, perturbations from Jupiter and Saturn have the

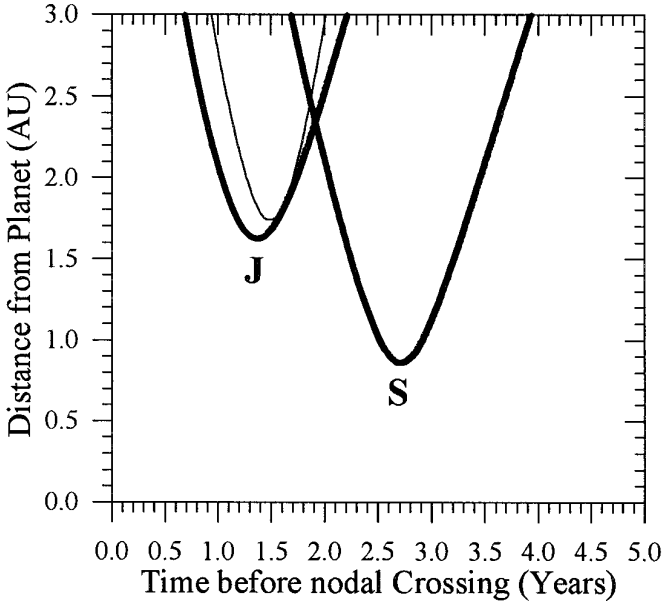

FIG. 12. Closest approach distances between the mean Perseid orbit (taken as the osculating orbit of 109P at its 1862 perihelion passage) and the planets Jupiter and Saturn shown as bold lines as a function of the time before nodal passage. The change in distance between Jupiter and a typical Perseid meteoroid is also shown (thin line).

largest effects on the semimajor axis of the orbit with increasingly smaller effects on e and the argument of perihelion, respectively.

In an encounter between a planet (in this case Jupiter or Saturn) and a Perseid meteoroid on a retrograde orbit crossing the planet's orbit above the ecliptic plane with dominant motion perpendicular to the planet's orbit and inward, the impulse is always a positive one and increases the energy of the associated meteoroid. The result of this effect is that the impulse delivered by Jupiter and Saturn produces a net inward shift in the node of perturbed Perseids. This shift results from the fact that the perturbation decreases the effective semimajor axis of the orbit and thus the first term in Eq. 12 (dR_d) is negative. Physically, the effect can be understood once it is seen that the encounter with either Jupiter or Saturn will rotate the velocity vector toward the ecliptic plane. It is precisely this effect that causes the inward shift of the node of meteoroids visible in Fig. 3 by a maximum amount of approximately 0.01 AU. It is not possible to use an Opik-like (or two-body) formalism to describe this encounter with Jupiter as the closest approach distance is almost 5 Hill Sphere radii from Jupiter and the impulse occurs over an extended region where the meteoroids' heliocentric velocity changes appreciably (cf. Greenberg *et al.* 1988 for a discussion of two-body encounters).

We have investigated this effect through numerical simulation and find that virtually all of the impulse causing this change occurs during the short interval of approximately ~1 year on either side of the closest approach to the planet. To verify that this encounter causes the observed nodal shift, we used 5000 test Perseid meteoroids ejected in 1862 and stopped the integration in 1986, mid-way between jovian perturbations (1979 and 1991). We then used these new elements as starting orbits, where each particle was followed with the direct perturbation term for Jupiter present and with it absent. All particles were followed to their descending nodes and the results of the perturbed and unperturbed final orbits compared. In all cases we found the perturbed meteoroids arrived at the node after the unperturbed meteoroids and with smaller nodal radii in the intervals nearest the jovian closest approaches. The energy difference between perturbed and unperturbed meteoroids in this simulation was greatest for particles having the largest jovian perturbations, with particles passing closest to Jupiter always having larger energies than the equivalent unperturbed trajectories. Figure 13 shows the relative energy difference between meteoroids experiencing close approaches to Jupiter relative to those which do not. Note that the local maximum near 2008 is an artifact owing to inclusion of the perturbations from Saturn during its 2006 close approach to the stream.

The magnitude of the perturbation in nodal radius is almost exactly the same for Jupiter as for Saturn, the net gravitational impulse for closest approach Perseids being identical owing to the closer distance of approach to Saturn (1.77 times) and slightly longer impulse time (for Saturn perturbations) precisely compensating the factor of 3 lower mass for Saturn.

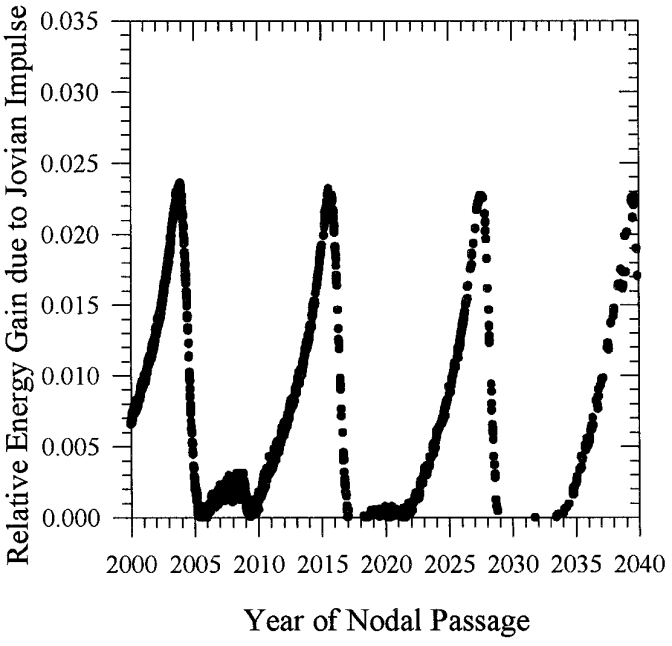

FIG. 13. Change in the relative energy of jovian perturbed and unperturbed Perseid meteoroids as a function of the time of their nodal passage.

Since 109P/Swift–Tuttle has had a nodal point outside the Earth's orbit for the past several thousand years, most meteoroids from these recent ejections are not accessible to Earth. On average, we have found that for our simulations the mean effect of radiation pressure is to move the node further outward, though this is not strictly the case for any one Perseid meteoroid, the final difference being a function of the initial ejection distance, velocity, and subsequent planetary perturbations for any given test particle. Only impulsive perturbations from Jupiter and Saturn can cause enough change in nodal distance for recently ejected meteoroids to make them visible from Earth.

This effect should produce noticeable changes in the activity of the stream for a short interval in solar longitude every 12 and 30 years as a result, which may persist for several years. This activity may be further heightened by the "focusing" effects of the perturbation, which concentrates the otherwise scattered nodal points of individual meteoroids, a direct result of the impulsive effects being larger than the smearing effects of initial ejection velocity and ejection geometry for recent ejecta. Indeed, Denning (1923) examined the then available records of the stream back to ancient times and concluded that a dominant period of 11.72 years best fit observations. Lindblad and

TABLE VI
Dates of Closest Approach between Jupiter and Saturn and the Perseid Stream over the Interval 1860–2050

Jupiter closest approach Date (YY/MM/DD)	Saturn closest approach Date (YY/MM/DD)
1860/9/15	1889/1/1
1872/7/26	1918/6/13
1884/6/5	1947/11/21
1896/4/18	1977/5/4
1908/2/27	2006/10/8
1920/1/7	2036/3/24
1931/11/17	
1943/9/27	
1955/8/7	
1967/6/17	
1979/4/26	
1991/3/6	
2003/1/14	
2014/11/24	
2026/10/4	
2038/8/14	

Porubcan (1994) investigated the solar longitude distribution of past photographically observed Perseids and concluded that the present outburst maximum was detectable as early as 1950. It is interesting to further note that on the basis of the present simulations we expect that some enhanced activity associated with the outburst portion of the stream should have been most apparent in the years near 1921, 1933, 1945, 1951, 1957, 1969, and 1980 with the maxima in 1921, 1945, 1957 and 1980 most prominent. Kronk (1988) lists the years 1920, 1931, 1945, and 1976–1983 as unusual for their reportedly high activity, while Grishchenyuk and Levina (1992) found evidence for extraordinary Perseid returns in 1921, 1956, 1980, and 1991. Given the vagaries of moonlight and sparse observer distributions in these periods, there appears to be a remarkable concordance between the two lists. It is particularly noteworthy that several other studies of the 1980 Perseid return, in particular, suggest enhanced activity, such as that of Russell (1990) who suggested on the basis of his photographic observations that the 1980 Perseids may have been particularly prone to fragmentation and hence of recent origin. Simek (1987) summarized nearly 30 years of radar observations of the Perseids and found that the 1980 return was the strongest recorded from 1958 to 1985 (with all the years from 1962 to 1972 having no observations), while Bel'kovich *et al.* (1995) determined that the returns from 1980 to 1982 were the strongest as recorded visually over the interval 1972–1990 from the former Soviet Union.

The close approaches by Jupiter and Saturn to the stream and an observed inward shift in the nodal positions of meteoroids show a lag of 1–3 years and a comparable duration (see Fig. 3). Table VI lists the dates of close approach to the stream by Jupiter and Saturn over an interval of one century.

The idea that the position of the planets might affect the observed shower activity on Earth is not new. Guth (1947) suggested that some showers were prone to increases in activity when the stream's orbit was in conjunction with a major planet. More recently, Jenniskens (1997) has shown that many streams show outbursts preferentially when the positions of Jupiter and Saturn are near conjunction with the stream. We would suggest that in these cases an impulse effect similar to the one found for the Perseids is also at work.

5.2. Geocentric Radiant Distributions—Theoretical vs Observed

The distribution of the theoretical radiants for the full 2000 and 100,000 year integrations are shown in Figs. 14 and 15 for photographic sized meteoroids ($10 < m < 0.1$ g). The temporal change in the rms width of the cumulative radiant distribution as a function of time for both orbit 1 and orbit 2 is shown in Fig. 16. The radiant dispersions for older ejections were approximated by weighting each geocentric radiant from an older ejection by the time between the next most recent and next older ejection in the model divided by the mean period of the comet within

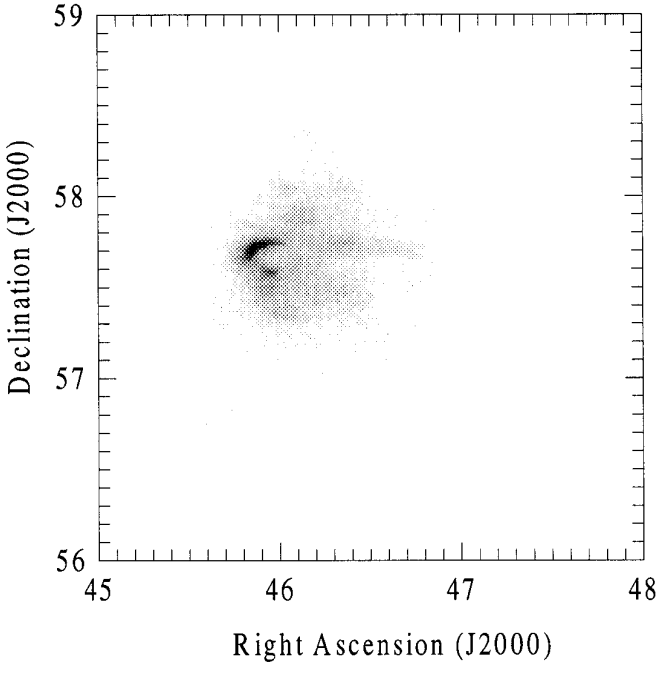

FIG. 14. Geocentric radiant distribution for all Earth-intersecting Perseids ejected from 59 to 1862 AD at the present epoch for photographic-sized meteoroids (mass > 0.1 g) from Model 42. Grid resolution is 0.02°. The dynamic grayscale range for this binning is from 0 to 320.

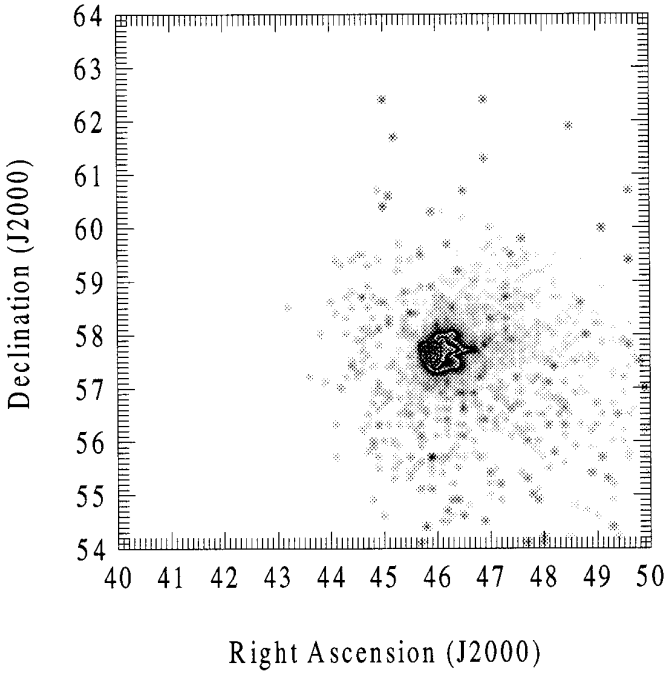

FIG. 15. Geocentric radiant distribution for all Earth-intersecting Perseids ejected over the past 100,000 years at the present epoch for photographic-sized meteoroids (mass > 0.1 g) for Model 42. The dynamic grayscale range for this binning is from 0 to 350.

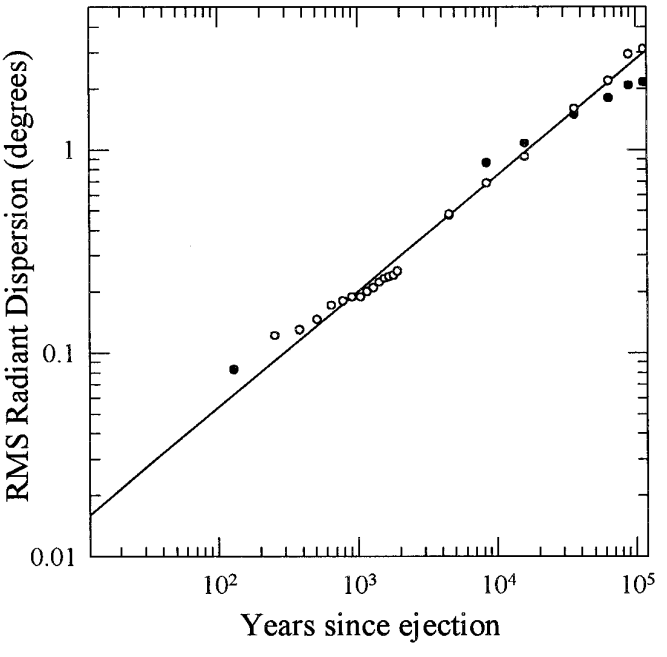

FIG. 16. Change in the rms width of the Perseid radiant for cumulative ejections over the past 100,000 years for seed orbit 1 (filled circles) and seed orbit 2 (open circles).

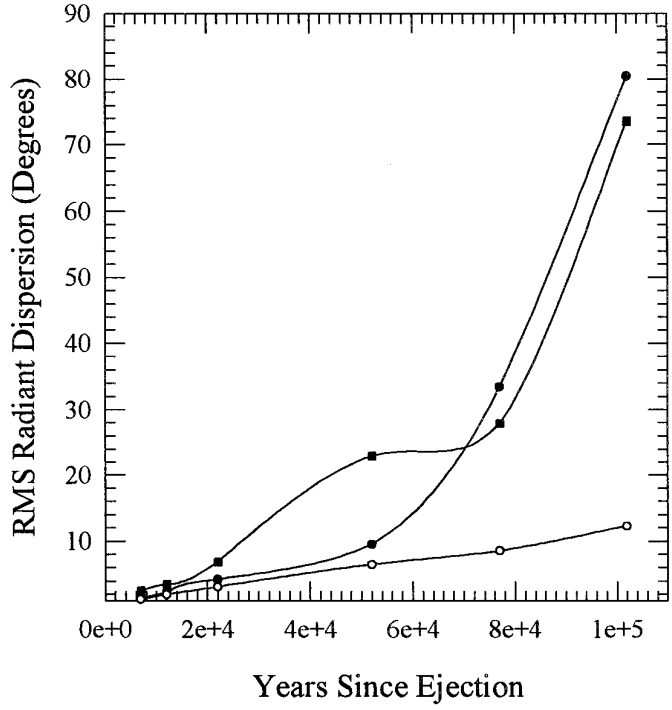

FIG. 17. Radiant dispersions for individual ejections of photographic-sized meteoroids from 5000 to 100,000 years ago for Perseids in the premaximum period ($\lambda_0 < 139°$) (solid circles), the maximum period ($139° < \lambda_0 < 140.3°$) (open circles), and in the post-maximum region ($\lambda_0 > 140.3°$) (solid squares).

that interval. While some difference exists between the dispersions found from orbits 1 and 2, the most consistent relation for the dispersion of the Perseid radiant over the full 100,000 years using the average of both orbits is

$$W = (4.74 \pm 0.84) \times 10^{-3}\, Y^{0.55}, \qquad (13)$$

where W is in degrees and Y is in years. The exponent in this power-law is very close to the 0.5 which would be expected for the case of random-walk-type diffusion.

The observed radiant dispersion for the Perseids changes as Earth passes through the stream. Kresak and Porubcan (1970) investigated the radiant of the stream using 250 photographed Perseids. They found the radiant showed a significant change in size across the stream, with the average dispersion being 1.39° for $\lambda_0 < 139°$, 1.10° for $139° < \lambda_0 < 140.3°$, and 1.33° for $\lambda_0 > 140.3°$. A more recent examination of the same question by Lindblad and Porubcan (1995) revealed a similar trend. While this trend is often interpreted as suggestive of older material outside the core portion of the stream, an observation supported by our findings, it is also significant that material further from the core of the stream is more likely to have been affected by planetary perturbations and is thus more dispersed. Figure 17 shows the dispersion at the present epoch

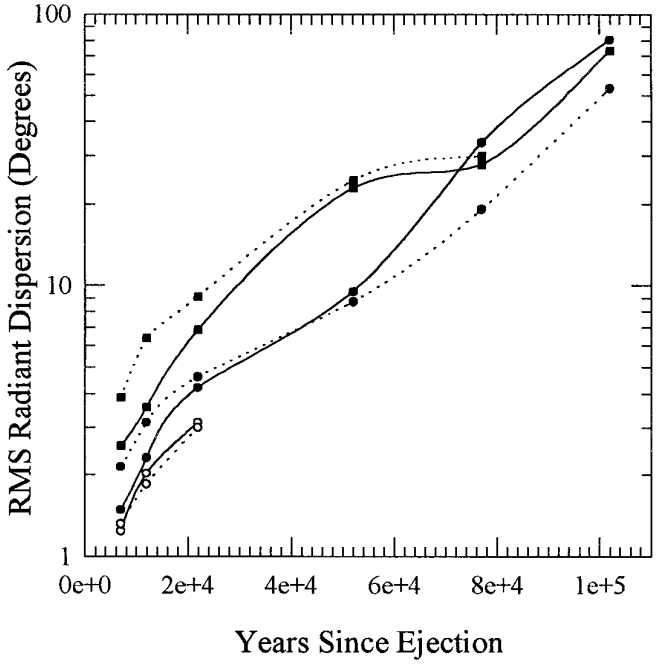

FIG. 18. Radiant dispersion of faint visual and radar class meteoroids (dotted line) as compared to brighter photographic Perseids for ejections from 5000 to 100,000 years ago. Symbols have the same meaning as in Fig. 17, and only ejections with at least 20 representative Earth-intersecting members at the present epoch are included.

for individual ejections in the intervals before, during, and after the main maximum. It is clear there is a large increase in dispersion away from the core of the stream for ejections of the same age.

Whipple and Wright (1954) noted a strong correlation between the nodal width (duration of activity) of a stream and radiant dispersion. They also noted the change in scatter as a function of mass should indicate whether physical forces such as initial ejection velocity and radiation effects are dominant over planetary perturbations. In Section 4.2 it was shown from an examination of visual-sized meteoroid radiant spreads from all models over the past 2000 years that the absolute rms size of the radiant is dominated for the first few revolutions by the initial ejection velocity and is later affected by radiation pressure in the longer term, whereas the rate of change of the radiant size is similar for all initial ejection conditions and densities of meteoroids and hence controlled by planetary perturbations (see Fig. 6). In Fig. 18, the radiant dispersion for faint visual and radar class meteoroids ($10^{-3} < m < 10^{-5}$) is shown for comparison to the photographic class meteoroids from the same models for orbit 2. In general, the radiant dispersion at present from any past ejection over this period tends to be greater for the smaller meteoroids than for the larger meteoroids, but the variation of the change between the two mass categories is similar for each period of activity of the stream. This supports the earlier conclusions of Section 4.2.

Lindblad and Porubcan (1995) found that the radiant area increased as the magnitude of the photographic Perseid decreased. Porubcan (1973) found the telescopic radiant spread of the shower to be significantly larger than the photographically determined width. All of these observations are consistent with our results showing the radiant spread to generally be larger at the present time for smaller meteoroids.

The average position of the geocentric radiant for photographic sized meteoroids from ejections over the past 2000 years is at $\alpha = 46.1° \pm 0.1°$ and $\delta = 57.66° \pm 0.05°$ referenced to J2000.0 and solar longitude 139.7°. This compares well to the location of the ''new'' component of the stream (outburst portion) found by Lindblad and Porubcan (1995) at $\alpha = 46.85° \pm 1.8°$ and $\delta = 57.6° \pm 0.99°$.

5.3. Progression Rate of the Node

The orbit of the Perseids and Swift–Tuttle are retrograde, hence the secular perturbations on the stream due to the planets result in a positive increase in the nodal longitude for the shower and the comet.

The change in position of the peak of the stream has been examined from ancient records by Hughes and Emerson (1982). They find that since 36 AD the node of the stream has advanced at an average rate of $(3.8 \pm 2.7) \times 10^{-4}$ degrees/year on the basis of the reported times of observation of the shower.

To derive a theoretical value for this number, we determined the position of the maximum of ejecta for each mass category at the current epoch for all ejections over the past 2000 years for all models. The slope of this distribution through time is found to be remarkably independent of mass—all masses were found to have an annual nodal progression rate well represented by

$$\frac{d\lambda_0}{dt} = (2.2 \pm 0.2) \times 10^{-4} \text{ degrees/year.} \qquad (14)$$

Figure 19 shows the distribution of maxima as a function of time for 0.01 g Perseids over the past 2000 years.

This nodal progression rate is an order of magnitude larger than the rate found over the interval from $5000 < t < 100{,}000$ years ago (Section 4.3). It is possible that the actual progression rate was lower in the distant past as the progression rate might decrease as we move backward in time if Swift–Tuttle's inclination more closely approached 90°. We note, however, the value for the progression rate at present to be most affected by recent ejections shown to be far more concentrated than older ejections and also more efficient at transporting Perseids into Earth-intersecting orbits as the comet's orbit probably passes closer to the Earth than it did in the past.

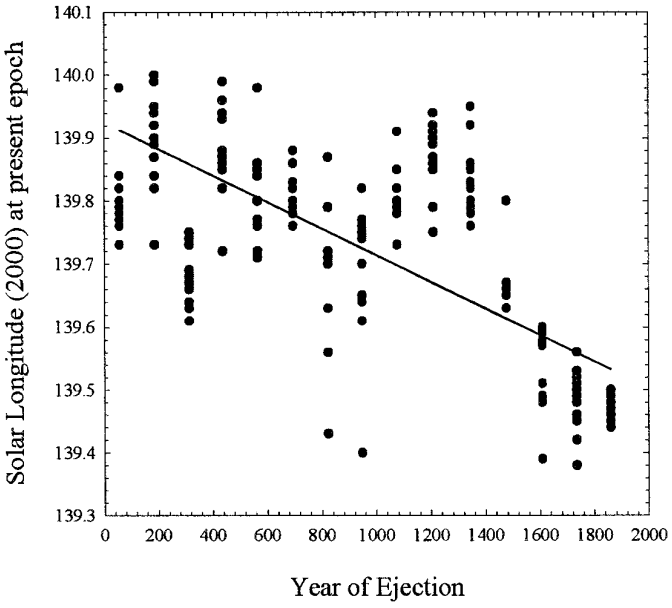

FIG. 19. Location of the maximum in activity as a function of solar longitude at the present epoch for individual ejections of 0.01 g Earth-intersecting Perseids over the past 2000 years. The results from all models have been included and each determination of the maximum location for each ejection epoch is represented by a dot. The line of best fit is also shown.

The theoretical progression rate we find is consistent with the Hughes and Emerson (1982) value.

5.4. Age of the Stream

The age of the Perseid stream remains a major question. From the nearly perpendicular orientation of the orbital plane, no major perturbations on the parent comet or stream is encountered. From the recent passage of the comet, we know Swift–Tuttle is among the most massive of the Halley-family of comets. Further observations supporting the stream's great antiquity include its very long period of activity and large mass (Hughes and McBride 1989) estimated to be upward of 10^{17} g.

It can be readily inferred that the shower is much older than typical meteoroid streams simply from its long duration. Southworth (1963), for example, estimated the stream age to be less than 6000 years on the basis of the rate of change in observed elements of photographic Perseids. In the other direction, Katasev and Kulikova (1975) noted that the stream must be younger than the time it takes for Poynting–Robertson drag to cause the particles to collide with the Sun, on the order of 10^6–10^7 years for visual-sized Perseids. Very few additional attempts to determine the age of the stream have been made.

From the modeling output there are several methods we can employ to estimate the age of the stream.

First, we may use the "average" radiant dispersion and Eq. (13). Kresak and Porubcan (1970) found the mean width of the radiant throughout its period of activity to be 1.27°. This yields an age estimate of $(30 \pm 10) \times 10^3$ years. From a data set with nearly double the number of Perseids, Lindblad and Porubcan derived a mean angular dispersion of 1.84° for the entire activity period of the shower, which corresponds to an age estimate of $(55 \pm 20) \times 10^3$ years. We note that in both cases these ages represent upper limits as the effects of individual radiant errors are not taken into account in these analyses and thus the true radiant rms spread is smaller than these values.

For the central portion of the stream we attempted to make a direct age estimate on the basis of the current position of the main, visual maximum (139.96 ± 0.04°). This was done by summing the activity from each ejection and with each additional passage, the location of the secondary peak in activity (corresponding to the broad maximum, as opposed to the outburst maximum) was found. Here we defined such a submaximum to be present if the peak in number of test meteoroids in any interval of 0.01° of solar longitude was above the number in all bins between 0.05° before and 0.05° after the position of the local maximum. By doing this for all 15 ejections from 59–1862 AD we noticed a slight shift in the position of this maximum as more ejections were added to the total. By assuming the geometry of encounter with Swift–Tuttle has remained reasonably similar to the average over the past 2000 years for the past ~10,000 years (a fact supported by our long-term integration of the comet's orbit in 4.3) we can then use this rate of shift, averaged for all models, to extrapolate to the number of total ejections needed to produce a peak at 139.96° at present. This procedure was done for all models and the position of the secondary maximum (found to move from approximately 139.7°–139.75° over the whole 2000-year period) as a function of the number of ejections added to the total (or equivalently the time) was determined. We note that this produces a lower limit as older ejections add less meteoroids to the core portion of the present population (all other things being equal), and each new ejection causes less of a change in the peak position due to the large number of previously existing meteoroids. In this way, we find that the shift in maxima would equal the present location of the observed maximum after $(11 \pm 3) \times 10^3$ years.

We can also use the width of the ZHR profile at the present time and compare it to the width of the distributions found for each of the long-term ejections to derive a lower limit for the age of the central portion of the stream, since the width of the individual distributions at present will always be larger than the actual width from cumulative ejections. From Brown and Rendtel (1996), the FWHM of the Perseid profile is approximately 2.1 ± 0.1°. From Eq. (9), the ejections attain this width after (14 ±

7) $\times 10^3$ years, implying that the age of the central portion of the stream must be >7000 years.

The absolute location in (α, δ) of the new and old components of the stream can also be compared with the rate of change in these elements with the weighted cumulative distribution location for the same elements to derive two approximate estimates for the age. Lindblad and Porubcan (1995) have shown that the average radiant location (referenced to $\lambda_0 = 139.7°$ (J2000.0)) is located at $\alpha = 47.52°$ and $\delta = 57.96°$ (from their Eqs. (1) and (2)). From the cumulative distributions over the past 2000 years averaged over all models and referenced to the same solar longitude, the change in right ascension is well represented by

$$\alpha = (45.88 \pm 0.01) + (1.13 \pm 0.03) \times 10^{-4}\, Y. \quad (15)$$

This yields an estimate of $(15 \pm 1) \times 10^3\ Y$ years for the age of the central portion of the stream.

For the location of the "average" declination for the stream, there is considerably more scatter in the slope of best-fit to the theoretical distribution because the secular variation in the declination is so small in comparison to amplitude variations caused by planetary perturbations.

An approximate expression averaged over all models is

$$\delta = (57.66 \pm 0.01) + (9.3 \pm 3.8) \times 10^{-6}\, Y, \quad (16)$$

which yields a median estimate of $\sim(38 \pm 16) \times 10^3$ years. Taken together these two determinations suggest an age of 15,000–20,000 years as most appropriate.

The above estimates represent the effective age of the majority of the photographic/visual-sized meteoroids in the Perseid stream. The age of the oldest meteoroids in the stream is much older, the amount of material from older returns having been diffused and hence not significantly contributing to the bulk of the currently visible core population. Perhaps the most effective means of gauging the total age of the stream is by comparing the full nodal spread of the current stream to the theoretical spread. The duration of the visibly detectable stream extends from roughly $\lambda_0 = 115$–$150°$ (Brown and Rendtel 1996) corresponding to calendar dates from mid-July to late August each year. There are hints that some activity from the shower must be visible outside this boundary (cf. Svoren *et al.* 1997), but the levels are lower than can be distinguished using visual observation techniques and we adopt the above as the minimum length of time the shower is presently active.

From Sections 4.2 and 4.3, the nodal dispersion from ejections at all visual-sized masses over the past 2000 years remains effectively contained within the region 139–140.5°. From Eq. (9), the Gaussian half-width from past ejections reaches this full width after nearly 180,000 years, though we caution that this is extrapolated well beyond the region where Eq. (9) was determined. If we take a "weak" level of observed activity to be possible even when the mean level of the theoretical activity is at a distance of 2σ from the peak, this would imply an overall age for the stream of ~90,000 years (roughly 700 orbital revolutions of the comet).

5.5. Long-Term Effects of Terrestrial Perturbations

Since the earliest recognition of the Perseids in the nineteenth century, the question of the role of Earth in the development of the stream has been posed by a number of authors (cf. Twining 1862, Shajn 1923). Previous works have examined the expected effects based on approximate analytic treatments of the average effect the Earth has on the stream, while ignoring the true physical character of the stream as a collection of many individual particles.

In an effort to address this question directly, we re-did all long-term integrations using seed orbit 1 with every condition identical, except that the direct planetary perturbation from the Earth was removed. We expect, a priori, that the influence of the Earth will be detected through an increase in the scatter of the orbital elements, particularly, a, i, and Ω in the simulation set containing the Earth as compared to the set without the Earth. The results show that in overall terms the Earth does have a perceptible effect on the evolution of the stream, but it is not more than a secondary influence in absolute terms.

That the Earth affects the stream is most evident in the width of the final nodal distributions as shown in Fig. 20. Here the difference between the Gaussian fit-widths between the final ejections with Earth and without are presented. The influence of the Earth is to add ~10% to the total width of the stream for those points containing the largest number of test particles. Similarly, the radiant dispersion increases by ~10% for any given age of ejection with inclusion of the Earth.

The terrestrial effect on the orbital element dispersions is shown in Table VII. Here the difference in the rms dispersion in the distribution of a, i, and ω for the No Earth–Earth simulations is given as well as the total number of meteoroids used in each distribution. There is a distinct tendency for the dispersions to be lower for the simulation with the Earth removed (negative values); however, the effect is far from universal. Particularly for the oldest ejections where fewer particles are involved, the statistical noise overwhelms the relatively small effect of the Earth's perturbations.

When the number of hyperbolically ejected Perseids is examined as a function of time (see Section 5.6 for more details) in comparison to the number lost without the Earth there is no statistical difference found between the two distributions at all masses. This attests to the dominance of Jupiter in ejecting Perseids from the Solar System. Curi-

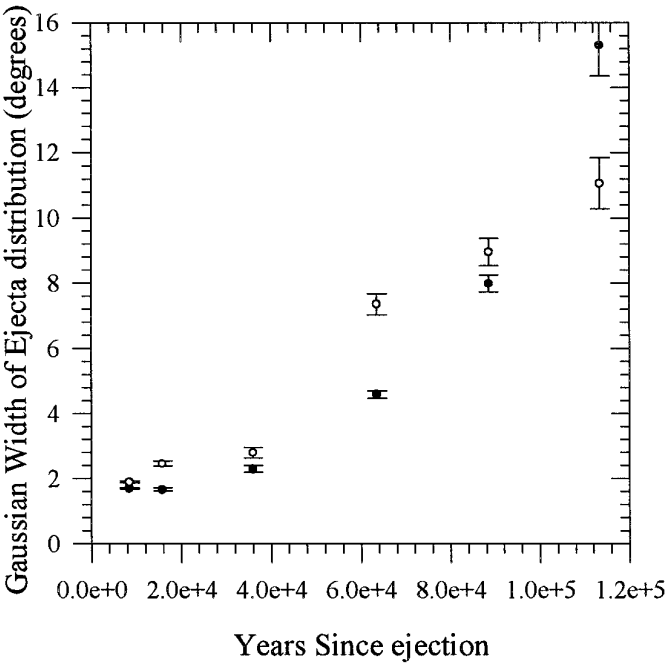

FIG. 20. Width of the final nodal distribution for Earth-intersecting Perseids for orbit 1 with the Earth (open circles) and without the Earth (solid circles).

ously, the same comparison of the number of Perseids lost due to attainment of a sungrazing state does show a noticeable difference. With the Earth removed, it is found that the number of sungrazing states reached is lower for the first 50,000–60,000 years after ejection. The difference is most striking for the smallest mass, where there is a much larger number of sungrazers for all times after ejection right up to 10^5 years. This effect is shown in Fig. 21, where the number of sungrazing Perseids is plotted against the year since ejection for simulations with and without the Earth. The Earth plays a more direct role in bringing Perseids to sungrazing states, possibly through the effects of close approaches.

5.6. Sinks for Stream Meteoroids: Sungrazers and Hyperbolic Ejection

It is usually assumed that the major sink for the Perseid stream is hyperbolic ejection due to planetary perturbations. The effect of collisions in removing meteoroids from the stream has been investigated in detail by Steel and Elford (1986) and they find the survival lifetimes to be at least several million years for Perseid meteoroids, making this a negligible loss channel over the 100,000-year period of our study.

For the long-term integrations, particles were removed from further integration when either their semimajor axis exceeded 200 AU or their perihelia decreased below 0.1

TABLE VII

The Difference in Keplerian Element rms Dispersion of the Perseid Stream for Seed Orbit 1 Meteoroids at Their Descending Nodal Passage at the Current Epoch with and without the Earth Present in the Integrations

Ejection time (year)	Mass (grams)	Number of meteroids Earth (No Earth)	Semimajor axis (a) (AU)	Inclination (i) (degrees)	Argument of perihelion
5000	10	496 (466)	−0.01	−0.49	−0.11
	0.1	491 (471)	−0.14	−0.54	0.00
	0.001	444 (530)	+0.02	−0.53	−0.05
10000	10	400 (383)	+0.1	−0.09	−0.27
	0.1	370 (430)	−0.04	−0.16	−0.26
	0.001	367 (390)	−0.25	−0.8	−0.06
20000	10	253 (303)	−0.09	−0.5	+0.07
	0.1	255 (270)	−0.47	−0.89	+0.29
	0.001	243 (246)	+0.05	+0.42	+0.02
50000	10	198 (212)	−0.7	−0.86	−0.17
	0.1	183 (200)	−1.3	−2.85	−0.83
	0.001	189 (188)	+1.06	−0.18	+0.81
75000	10	87 (88)	+2.15	−2.88	−6.69
	0.1	91 (89)	−1.17	−2.45	+2.32
	0.001	84 (96)	−2.79	−2.68	+0.75
100000	10	40 (49)	−0.17	−3.77	+2.93
	0.1	70 (60)	+0.21	+0.91	+3.98
	0.001	72 (85)	−0.36	+0.41	+2.34

Note. The number of meteoroids for each sample is given (with the No Earth simulation in parentheses). The differences are $\sigma_{\text{No Earth}} - \sigma_{\text{Earth}}$. Negative values imply that the presence of the Earth makes the dispersion larger.

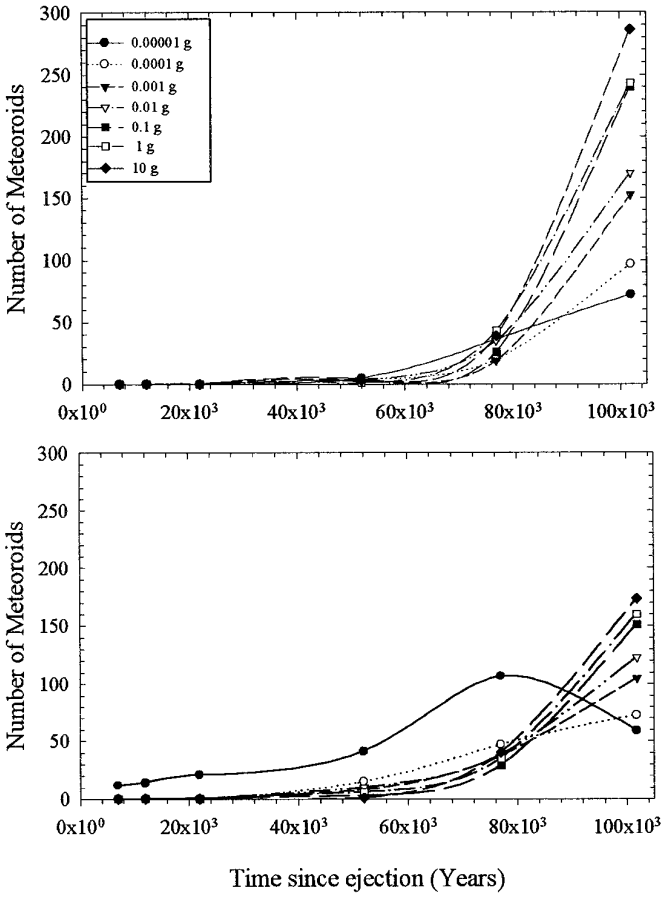

FIG. 21. Number of Perseid meteoroids which reach a sungrazing state as a function of time since ejection for simulation with the Earth present (bottom graph) and with it removed (top graph) for all 7 mass categories. The legend shows the symbol–mass correspondence.

AU, corresponding to a sungrazing end state. This latter removal condition is likely too strict as several annual meteoroid streams have perihelia inside this distance—the survivability of Perseids this close to the Sun is not known, but given the evidence from other streams suggests that our sungrazing (or near-sungrazing) conditions should be viewed as upper limits. For comparison, the cometary lexicon typically defines sungrazing states as orbits with perihelia of 0.01 AU or less (Bailey *et al.* 1992).

The fraction of Perseids removed in either of these ways varied dramatically between the long-term orbits 1 and 2. In particular, orbit 2 with a much larger eccentricity and semimajor axis showed an order of magnitude greater loss than orbit 1 for both loss channels.

The primary loss mechanism, especially for smaller meteoroids, was found to be hyperbolic ejection due mainly to direct perturbations from Jupiter with a minor contribution from Saturn. For both orbits 1 and 2, the hyperbolic loss tended to increase at smaller Perseid meteoroid masses, this effect being the result of radiation pressure which increases the average energy of the meteoroid orbit and leads to more losses. However, for orbit 1 this trend was nearly reversed for ejections 10^5 years ago attesting to the importance of the cometary orbit at time of ejection and thus to the orbits accessible through planetary perturbations to meteoroids of differing ejection velocities. After 10^5 years the percentage hyperbolic loss for orbit 2 for radar-sized meteoroids (10^{-5} g) approached 35% of all ejected meteoroids. For comparison, only 1% of orbit 1 Perseids were lost in any given mass category due to hyperbolic ejection after 10^5 years. Figure 22 shows the number of ejected Perseids released at various ejections over the past 10^5 years for all masses for orbit 1 and 2 removed due to hyperbolic ejection before the present epoch.

Bailey *et al.* (1992) demonstrated that comets with orbits nearly perpendicular to the ecliptic plane and perihelion moderately close to the Sun (0–2 AU) are susceptible to sungrazing states. We have found that for larger Perseids ($>10^{-3}$ g) and for both orbit variations used here, our near-

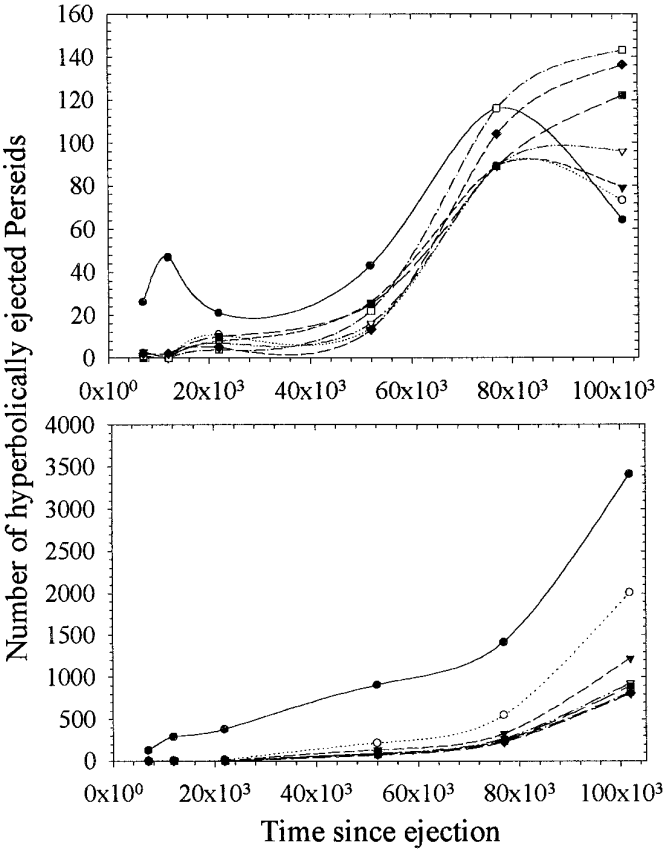

FIG. 22. The number of hyperbolically ejected Perseid meteoroids as a function of year since ejection from the parent comet for orbit 1 (top graph) and orbit 2 (bottom graph) meteoroids. The symbol–mass correspondence is the same as Fig. 21.

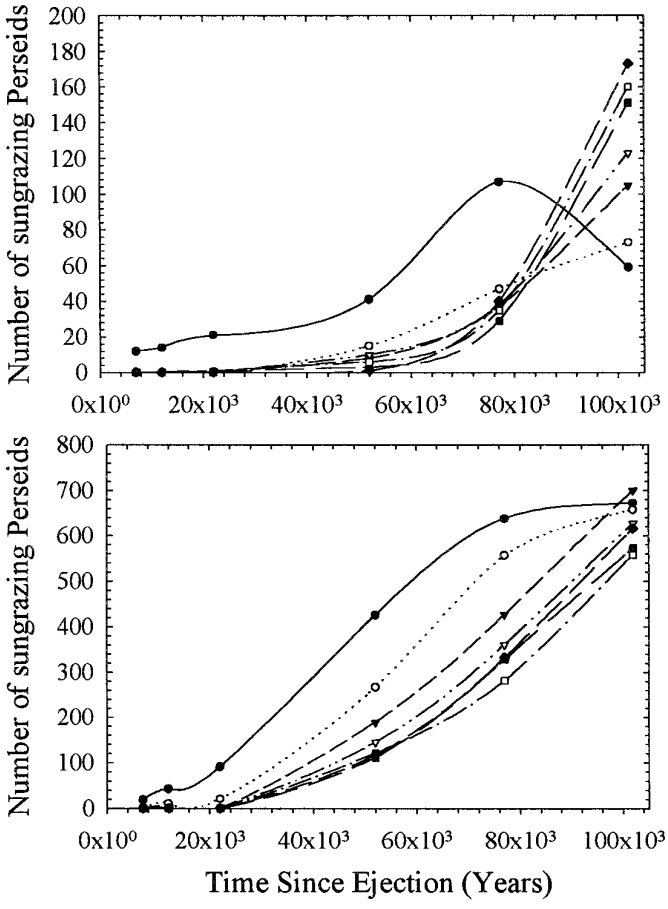

FIG. 23. The number of Perseids that enter sungrazing states as a function of time since ejection from the parent comet for orbit 1 (top graph) and orbit 2 (bottom graph) for all 7 mass categories. The symbol–mass correspondence is the same as Fig. 21.

sungrazing end state can be almost as efficient as hyperbolic ejection (and in some cases more so) as a sink for the stream. Figure 23 shows the number of Perseids that enter sungrazing states as a function of ejection time for orbits 1 and 2. The same mass dependence is found as for hyperbolic ejection, with the smallest Perseids being preferentially removed.

The length of time needed for meteoroids to enter either of these states depends primarily on the comet orbit adopted (which changes significantly from one ejection epoch to another) used for initial ejection from Swift–Tuttle and to a lesser extent on mass. For all but the smallest mass category, the average time taken before any significant number (>10) of Perseids are thrown onto hyperbolic orbits is 40,000–60,000 years for both seed orbits. For sungrazing orbits, the time taken to reach this state falls in the range from 10,000–80,000 years, with an average near 60,000 years. The slope of the number of meteoroids lost as a function of time for either loss channel varies between the two seed orbits, between masses, and times of ejection. In general, a linear or quadratic increase in the number of meteoroids lost is a good representation of the distribution after the initial loss time (as given above), with photographic-sized meteoroids being lost at a peak rate of 1–5 every revolution of the comet (corresponding to 0.01–0.05% of the number of total meteoroids initially ejected) after this time from any one mass category due to hyperbolic ejection. This implies a lower limit for the removal time of 50% of the largest particles due to attainment of hyperbolic orbits of ~200,000 years after their initial ejection. The removal rate resulting from entry into a sungrazing state is comparable to this value for the largest meteoroids. The actual removal time is typically at least several times larger than this lower limit (depending on mass) based on our integrations, with some combinations of initial seed ejection orbit and masses showing loss rates which correspond to survival times almost 2 orders of magnitude longer than this lower limit.

From all of the above considerations it is apparent that a Perseid meteoroid can, on average, survive for a minimum of several 10^5 years before being removed by one of these loss mechanisms, thus testifying to the possible large age of the stream, which we believe to be limited only by the capture time of Swift–Tuttle.

6. FUTURE ACTIVITY OF THE PERSEIDS

If the modeling results presented here are representative of the true Perseid stream, then some predictions of the time and strength of the activity of the stream for the next several years may serve to validate the model. Table VIII gives the predictions of the peak time and strength for the outburst maximum for the Perseids from 1997 to 1999. The composition of each of these outburst maxima, in terms of the fraction of encountered meteoroids from the three most significant perihelion passages of Swift–Tuttle, summed over all models, is also presented. If the locations of maximum and levels of activity are found to be in good agreement with observations over the next few years, this will present the opportunity to record Perseid meteoroids whose ejection origin is well known and for which precision observations would be most valuable as a result.

Over the longer term, Fig. 5 shows that the activity of the Perseids is expected to wax and wane and that the strength of the outburst maximum should be quite variable over the coming years. In particular, a minimum in annual activity from the outburst portion of the stream might be expected circa 2001–2002 and a subsequent revival in 2004–2006. The latter increase in activity would be the direct result of the close approach to stream meteoroids by Jupiter early in 2003.

TABLE VIII

Future Peak Times of the Outburst Portion of the Perseid Stream and Approximate ZHRs (Scaled to a Normal Perseid Peak ZHR of 86 ± 1) for the Outburst from 1997 to 2000

Year	Weighted location of maximum (J2000)	Contributing ejection epochs	Estimated ZHR of outburst maximum
1997	139.68 ± 0.04	1479 (0.31) 1079 (0.17) 0826 (0.14)	95 ± 6
1998	139.73 ± 0.05	1079 (0.20) 0826 (0.14) 1479 (0.11)	111 ± 6
1999	139.76 ± 0.05	1079 (0.18) 0826 (0.16) 0698 (0.13)	115 ± 8

Note. The ejections contributing to the activity are also shown along with the total fraction of meteoroids in that year from a particular ejection epoch. Note that according to Arlt and Rendtel (1997) the 1997 Perseid peak occurred at 139.72° with an outburst ZHR of 137 ± 7 and a normal peak ZHR of 105 ± 6 at 140°. Scaling our 1997 theoretical value using this observed normal peak ZHR in 1997 gives a predicted outburst ZHR of 116 ± 15.

7. CONCLUSIONS

From the analysis of the results of numerical modeling of the stream we may draw several conclusions pertinent to the opening questions presented in the Introduction:

1. The initial ejection conditions play a central role in the final observed distribution of Perseid meteoroids at the Earth over time scales on the order of ~5 cometary revolutions. After this interval, the effects of planetary perturbations and radiation forces begin to dominate the subsequent evolution of the stream, an effect which is manifested in the changing radiant size at present as a function of the time since ejection and by the lack of difference in the relative final activity as seen from Earth due to all the different ejection models from older ejections.

The choice of sun-centered cone angle makes only a marginal difference to the final activity outcomes. Different cone angles produce small changes to the total length of time overwhich activity occurs in any one year, particularly for recent ejections, with larger cone angles associated with longer activity. Narrower cones also limit the range of masses of Perseids subsequently accessible to Earth for more recent ejections.

From the model outputs, dust ejected at larger distances from the Sun has a very minor effect on the final activity of the stream observed from Earth. The primary reason for this is the assumption of uniform ejection over the allowable range of true anomalies which automatically concentrates the majority of the ejections close to perihelion. The outlying dust tends to end up on the periphery of the overall nodal longitude distributions (see Fig. 11).

The density assumed for the meteoroids has the largest effect on the final distributions. That the evolutionary path is so sensitive to the assumed density of the particles is apparent by the systematic and consistent change in the number of meteoroids observed at Earth within each model as density is changed (cf. Table II). In particular, the number of meteoroids encountered increases with increasing assumed density. The change in density is related to both the ejection velocity and radiation pressure (both values increasing with decreasing density). However, since 109P/Swift–Tuttle's descending node has been outside Earth's orbit for the past 2000 years, all meteoroids destined to encounter the Earth must be perturbed inward. Higher ejection velocities allow some meteoroids to have osculating orbits at ejection with nodal radii lower than the parent comet. If no other forces influenced the meteoroids we would expect to see more low-density Earth-intersecting meteoroids (which have higher ejection velocities); the opposite trend is observed. This is a direct result of radiation pressure moving the meteoroidal nodal point further out from the Sun and this force being greater for the lower density particles, as confirmed directly in Section 5.1. This effect dominates over the inward nodal motion caused by the initial ejection velocity dispersion.

In using observations to constrain the model output, radiant location and orbital element distributions were found to be subject to measurement errors substantially larger than those intrinsic to the actual physical dispersions predicted by all models investigated. A quantitative assessment of the goodness of fit between the observed and predicted peak flux of the outburst portion of the stream

and the location of the outbursts for the years 1989–1996 demonstrated that Models 22 and 21, respectively, provided the best overall fit. The lowest ejection velocity model (Model 1—distributed production) showed significantly poorer fits to the flux than the other models. This suggests that very low ejection velocities (few m/s to a maximum of a few tens of m/s) are not representative of the decay process associated with Swift–Tuttle and that the density of meteoroids associated with the outburst portion of the stream is on the order of 100–1000 kg m^{-3}.

At the other extreme, the very high ejection velocities recently proposed to explain the distribution in semimajor axes within the stream by Harris and Hughes (1995) and Williams (1996) are also not consistent with the observations. In particular, by using such high ejection velocities (0.6 km/s near perihelion), it was found that the geocentric radiant dispersion from 1862 would be greater than 0.5°. Our results (see Fig. 6) suggest that ''normal'' ejection velocities from 1862 would produce radiant dispersions close to 0.1° at present. From our simulations, the Perseid outbursts from 1991 to 1994 consist primarily of material ejected in 1862. Shiba *et al.* (1993) report photographic observations of the 1991 outburst showing a radiant dispersion of ~0.1° from seven of nine photographed Perseids, while Spurny (1995) reports that the radiant dispersion for the 1993 outburst was 0.3° for the concentrated portion (13 of 19 recorded Perseids) during that outburst. As individual radiant errors have not been incorporated into these measures, each of the observed dispersions represent upper limits, the true dispersions being smaller. As such, the ejection velocities we have employed appear to match the observed radiant sizes well, and at the same time they rule out the very high (~0.6 km/s at perihelion) ejection velocities proposed elsewhere. This is also consistent with our earlier remarks concerning the inadmissibility of orbital elements for the determination of original ejection velocities using current photographic techniques with the present size of their measurement errors.

2 and 3. The location of the outburst portion of the Perseid stream has changed position over the past 8 years due to a change in the age of the meteoroids found in this portion of the stream during that interval. From the simulation results, the outbursts from 1988 to 1990 were principally composed of meteoroids ejected in 1610 and 1737, while the 1991–1994 maxima consisted of material released in 1862 and 1610. The most recent outbursts (1995–1996) are from particles released in 1479 and 1079. The progressive relative increase in the location of the maximums in the years away from 1993 is due to the influence of the older ejections which were released from the parent comet at larger nodal longitudes than the comets current location and further increased due to secular perturbations.

The high activity from the stream, particularly in the years 1991–1994 is due in part to the return of Swift–Tuttle and the numerous meteoroids in the Perseid stream with very similar periods to the parent comet. This, however, is a necessary but not sufficient condition for the occurrence of the outbursts. An impulsive change inward of the nodal radius of the youngest portion of the stream due to a close approach to the stream orbit by Jupiter in 1991 was the additional condition sufficient to ensure that significantly enhanced activity from the shower occurred. This also explains the sudden onset in 1991; in the few years immediately prior to this time, meteoroids from 1862 were generally outside Earth's orbit and inaccessible to it as a result.

The discrepancy in the observed times of peak nearest Swift–Tuttle's perihelion passage (particularly in 1993 and 1994) can be explained by a strong asymmetry in dust production during the 1862 passage of Swift–Tuttle. In particular, observations from that epoch indicate a strong tendency for ejections to have a large component of their total velocity in the positive normal direction relative to Swift–Tuttle's orbit (i.e., perpendicular to the cometary orbital plane in a direction from which the comet appears to revolve counterclockwise). This tends to produce activity at Earth in the present epoch with nodal longitudes larger than the parent comet, and this can explain the difference between the (earlier) model predicted peak times and those observed nearest Swift–Tuttle's return when ejecta from 1862 predominated.

Our results also suggest that some smaller levels of ''outburst'' activity from the stream should have been visible well before the return of Swift–Tuttle as a result of the direct perturbations from Jupiter and Saturn. That no definitive visual observations of prior outbursts of the stream exist may be due to the fact that the first global synthesis of large numbers of visual observations of the stream did not occur until 1988. Thus, the appearance of an early maximum in that year may not be intrinsic to the stream, but only to the scrutiny with which it was observed. Perseid returns over the past 70 years do show years of stronger Perseid activity, and these years closely match those predicted assuming planetary impulsive effects are the root cause.

4. From comparison of the radiant size of the Perseid stream and our model estimates of the change in radiant dispersion with age, the photographic-sized meteoroids in the main core of the stream are approximately 40,000 years old. Using the rate of change in the apparent location of the maximum, a lower limit of 11,000 years is obtained for the core of the stream. Similarly, using the width of the ZHR profile of the stream compared to the theoretical estimates yields another lower limit estimate for the central portion of the stream of 14,000 years. The photographic radiant locations at maximum are reproduced in the modeling with ejections 15,000–20,000 years of age. These esti-

mates, along with their errors as given in Section 5.4, are most consistent with a core population of Perseids having mean ages on the order of $(25 \pm 10) \times 10^3$ years. It is instructive to note that from the long-term integrations in Section 4.3 of the parent comet, the most probable evolutionary paths for Swift–Tuttle all have nodal distances less than 0.1 AU from the Earth over the past 20,000 years, and we would suggest that it is the dynamics of Swift–Tuttle's orbit over the past 20–30 millennia that control the highest activity portion of the stream presently visible from Earth.

The long duration of the Perseid shower indicates that the total age of the stream is much older. Our integrations show that some activity from the shower may be detectable from Earth for a significant portion of the entire year if the shower is as young as 10^5 years. Given the currently accepted duration of the shower of 40–45 days implies a lower limit for the age of the stream on the order of 10^5 years. It is not possible to be more precise given uncertainties in the total length of time activity of the stream is visible from Earth and the precise evolutionary path followed by Swift–Tuttle.

A portion of our integrations suggests that if enough evolution occurs, some Perseid meteoroids may begin encountering the Earth at their ascending nodes in mid-March. Several candidate showers which are documented, but whose orbital elements are poorly known, have been identified. The existence of such a shower and positive association with Swift–Tuttle would imply a stream age of at least 50,000–75,000 years.

5. We find that the current nodal progression rate of the stream (averaged over all models and masses for the past 2000 years) is $(2.2 \pm 0.2) \times 10^{-4}$ degrees/year. This is in good agreement with the observed rate of change of the location of the peak of the shower in historical times found by Hughes and Emerson (1982) of $(3.8 \pm 2.7) \times 10^{-4}$ degrees/annum.

6. The Earth has a minor effect on the long-term evolution of the stream. In general terms, we have found that the Earth contributes approximately ~10% to the total nodal dispersion of the stream and increases the radiant dispersion by a similar amount over time scales of order many thousands–tens of thousands of years. The Earth's scattering effect on the stream is also visible in the rms spreads in the orbital elements (a, i, ω), with the rms scatter becoming smaller in these elements with the Earth removed. The effect is apparent in these orbital element dispersions, but far from dominant, with small number statistics become increasingly important for the oldest ejections. The Earth plays no perceptible role in moving Perseids into hyperbolic orbits, but does appear to play some role in shepherding Perseids into sungrazing states.

7. Two dynamical effects remove Perseids from the stream; hyperbolic ejection due to Jupiter (and to a lesser degree Saturn) and entry into sungrazing states. The relative importance and absolute amount of loss due to these mechanisms depends on the precise evolutionary path assumed for Swift–Tuttle and also varies by mass. The smallest Perseids tend to be preferentially removed first due to their lower average energies resulting from larger radiation pressure effects. The rate of removal varied dramatically between the two assumed seed orbits (and by mass) with as many as 35% of the initial Perseid population hyperbolically ejected after 10^5 years for small meteoroids using seed orbit 2, while seed orbit 1 produced a loss rate of 1% over the same interval. Typically, it required $40–80 \times 10^3$ years before any significant number (>0.1% of the initial population) was removed due to either of these two effects, but the actual number varied significantly from case to case.

8. The delivery of Perseid meteoroids into Earth-intersecting orbits is principally controlled by the evolutionary path of the parent comet. The closest approach distance between the osculating orbit of Swift–Tuttle at the time of release of the meteoroids and the number of Perseids visible at the present time is positively correlated over the past 2000 years. Over the longer term, the assumed starting orbit for the initial ejections critically influences the subsequent development and activity of the shower as seen from the Earth. In the short term, impulsive perturbations due to Jupiter and Saturn control the magnitude of the outburst component of the stream and thus the amount of relatively ''fresh'' Perseid material visible from Earth.

ACKNOWLEDGMENTS

The authors thank the National Science and Engineering Research Council of Canada for funding this work. P.B. acknowledges a scholarship provided by the Institute of Space and Terrestrial Science in support of this work. Helpful reviews by V. Porubcan and D. W. Hughes greatly enhanced the original.

REFERENCES

Arlt, R., and J. Rendtel 1997. First analysis of the 1997 Perseids. *WGN J. IMO* **25,** 207–209.

Babadzhanov, P. 1993. Densities of meteoroids. In *Meteoroids and Their Parent Bodies* (J. Stohl and I. P. Williams, Eds.), pp. 295–302. Astronomical Inst. Slovak Acad. Sci., Bratislava.

Bailey, M. E., J. E. Chambers, and G. Hahn 1992. Origin of sungrazers—A frequent cometary end-state. *Astron. Astrophys.* **257,** 315–322.

Bel'kovich, O. I., A. I. Grishchenyuk, M. G. Ishmukhametova, S. Levin, A. S. Levina, V. V. Martynenko, N. I. Suleimanov, and V. Yaremchuk 1995. The structure of the Perseid meteoric stream from visual observations during 1972–1993. *Solar System Res.* **29,** 473–477.

Boehnhardt, H., K. Birkle and M. Osterloh 1996. Nucleus and tail studies of Comet P/Swift–Tuttle. *Earth, Moon, Planets* **73,** 51–70.

Burns, J. A., P. L. Lamy, and S. Soter 1979. Radiation forces on small particles in the Solar System. *Icarus* **40,** 1–48.

Brown, P., and J. Rendtel 1996. The Perseid meteoroid stream: Characterization of recent activity from visual observations. *Icarus* **124,** 414–428.

Ceplecha, Z. 1988. Earth's influx of different populations of sporadic meteoroids from photographic and television data. *BAC* **39,** 221–236.

Ceplecha, Z. 1996. Luminous efficiency based on photographic observations of the Lost City fireball and implications for the influx of interplanetary bodies onto Earth. *Astron. Astrophys.* **11,** 329–332.

Ceplecha, Z., P. Spurny, J. Borovicka, and J. Keclikova 1993. Atmospheric fragmentation of meteoroids. *Astron. Astrophys.* **279,** 615–626.

Chambers, J. E. 1995. The long term dynamical evolution of Comet Swift–Tuttle. *Icarus* **114,** 372–386.

Combi, M. R. 1989. The outflow speed of the coma of Halley's comet. *Icarus* **81,** 41–50.

Crifo, J. F. 1995. A general physicochemical model of the inner coma of active comets. I. Implications of spatially distributed gas and dust production. *Astrophys. J.* **445,** 470–488.

Denning, W. F. 1923. Radiant points of shooting stars observed at Bristol chiefly from 1912 to 1922 inclusive. *Mon. Not. R. Astron. Soc.* **84,** 43–56.

Everhart, E. 1985. An efficient integrator that uses Gauss–Radau spacing. In *Proceedings of IAU Colloquium No. 83: Dynamics of Comets: Their Origin and Evolution* (A. Carusi and G. Valsecchi, Eds.), p. 185. Reidel, Dordrecht.

Festou, M. C., H. Rickman, and R. M. West 1993. Comets. 2: Models, evolution, origin and outlook. *Astron. Astrophys. Rev* **5,** 37–163.

Fomenkova, M. N., B. Jones, R. Pina, R. Puetter, J. Sarmecanic, R. Gehra, and T. Jones 1995. Mid-infrared observations of the nucleus and dust of Comet P/Swift–Tuttle. *Astron. J.* **110,** 1866–1874.

Guigay, M. 1947. Reserches sur la constitution du courant d'etoiles filantes des Perseides, J. Observateurs. *Comptes Rendus* **30,** 33–48.

Guth, V. 1947. On the Periodicity of the Lyrids. *BAC* **1,** 1–4.

Gustafson, B. A. S. 1989. Comet ejection and dynamics of nonspherical dust particles and meteoroids. *Astrophys. J.* **337,** 945–949.

Greenberg R., A. Carusi, and G. B. Valsecchi 1988. Outcomes of planetary close encounters: A systematic comparison of methodologies. *Icarus* **75,** 1–29.

Grishchenyuk, A., and A. Levina 1992. The reappearance of P/Swift–Tuttle. *WGN J. IMO,* **20,** 162–163.

Hamid, S. E. 1951. The formation and evolution of the Perseid meteor stream. *Astron. J.* **56,** 126–127.

Harris, N. W., and D. W. Hughes 1995. Perseid meteoroids—The relationship between mass and orbital semimajor axis. *Mon. Not. R. Astron. Soc.* **273,** 992–998.

Harris, N. W., K. C. C. Yau, and D. W. Hughes. 1995. The true extent of the nodal distribution of the Perseid meteoroid stream. *Mon. Not. R. Astron. Soc.* **273,** 999–1015.

Hasegawa, I. 1993. Historical records of meteor showers. In *Meteoroids and Their Parent Bodies* (J. Stohl and I. P. Williams, Eds.), pp. 209–227. Astronomical Inst. Slovak Acad. Sci., Bratislava.

Hughes, D. W. 1995. The Perseid meteor shower. *Earth, Moon, Planets* **68,** 31–70.

Hughes, D. W., and B. Emerson 1982. The stability of the node of the Perseid meteor stream. *The Obs.* **102,** 39–42.

Hughes, D. W., and N. McBride 1989. The mass of meteoroid streams. *Mon. Not. R. Astron. Soc.* **240,** 73–79.

Jacchia, L., and F. L. Whipple, 1961. Precision orbits of 413 photographic meteors. *Smith. Contr. Astrophys.* **4,** 97–129.

Jenniskens, P. 1994. Meteor stream activity I: The annual streams. *Astron. Astrophys.* **287,** 990–1013.

Jenniskens, P. 1997. Meteor stream activity IV: Meteor outbursts and the reflex motion of the Sun. *Astron. Astrophys.* **317,** 953–961.

Jones, J. 1985. The structure of the Geminid meteor stream. I—The effect of planetary perturbations. *Mon. Not. R. Astron. Soc.* **217,** 523–532.

Jones, J. 1995. The ejection of meteoroids from comets. *Mon. Not. R. Astron. Soc.* **275,** 773–780.

Katasev, L. A., and N. V. Kulikova 1975, Origin and evolution of the Perseid meteor stream. *Solar System Res.* **9,** 136–141.

Kresak, L. 1957. On the collisional hypothesis of the origin of the Perseid meteor stream. *Contr. Skalnate. Pleso* **2,** 7–19.

Kresak, L. 1976. Orbital evolution of the dust streams released from comets. *BAC* **27,** 35–46.

Kresak, L. 1992. On the ejection and dispersion velocities of meteor particles. *Contr. Skalnate. Pleso* **22,** 123–130.

Kresak, L., and V. Porubcan 1970. The dispersion of meteors in meteor streams I. The size of the radiant areas. *BAC* **21,** 153–170.

Kresakova, M. 1974. On the accuracy of semimajor axes of meteor orbits. *BAC* **25,** 191–98.

Kronk, G. W. 1988. *Meteor Showers: A Descriptive Catalog*. Enslow, New Jersey.

Lindblad, B. A. 1991. The IAU meteor data center in Lund. In *Origin and Evolution of Interplanetary Dust* (A. C. Levasseur-Regourd and H. Hasegawa, Eds.), pp. 311–315. Kluwer Academic, Dordrecht.

Lindblad, B. A., and V. Porubcan 1994. The activity and orbit of the Perseid meteor stream. *Planet. Space Sci.* **42,** 117–123.

Lindblad, B. A., and V. Porubcan 1995. Radiant ephemeris and radiant area of the Perseid meteoroid stream. *Earth, Moon, Planets* **68,** 409–418.

Levison, H. F., and M. J. Duncan 1994. The long-term dynamical behavior of short-period comets. *Icarus* **108,** 18–36.

Marsden, B. G., G. V. Williams, G. W. Kronk, and W. G. Waddington 1993. Update on Comet Swift–Tuttle. *Icarus* **105,** 420–426.

McDonnell, J. A. M., and 9 colleagues 1987. The dust distribution within the inner coma of Comet P/Halley 1982i—Encounter by Giotto's impact detectors. *Astron. Astrophys.* **187,** 719–741.

Nakamura, R., Y. Kitada, and T. Mukai 1994. Gas drag forces on fractal aggregates. *Planet. Space Sci.* **42,** 721–726.

O'Ceallaigh, D. P., A. Fitzsimmons, and I. P. Williams 1995. CCD photometry of Comet 109P/Swift–Tuttle. *Astron. Astrophys.* **297,** L17–L20.

Olivier, C. P. 1925. *Meteors*. Williams and Wilkens, Baltimore.

Porubcan, V. 1973. The telescopic radiant areas of the Perseids and Orionids. *BAC* **24,** 1–8.

Porubcan, V. 1977. Dispersion of orbital elements within the Perseid meteor stream. *BAC* **8,** 257–266.

Press, W. H., B. P. Flannery, and S. A. Teukolsky 1986. *Numerical Recipes. The Art of Scientific Computing.* Cambridge Univ. Press, Cambridge.

Rendtel, J., and R. Arlt 1996. Perseids 1995 and 1996—An analysis of global data. *WGN J IMO* **24,** 141–147.

Rendtel, J., R. Arlt, and A. McBeath 1995. *Handbook for Visual Meteor Observers.* International Meteor Organization, Potsdam.

Rickman, H. 1986. Masses and densities of Comets Halley and Kopf. In *Proceedings ESA Workshop: Comet Nucleus Sample Return SP-249*, p. 195. ESA, Canterbury.

Roy, A. E. 1978. *Orbital Motion*. Hilger, Bristol.

Russell, J. A. 1990. Dissimilarities in Perseid meteoroids. *Meteoritics* **25,** 177–180.

Sagdeev, R. Z., J. Kissel, E. N. Evlanov, L. M. Mukhin, B. V. Zubkov, O. F. Prilutskii, and M. N. Fomenkova 1987. Elemental composition of the dust component of Halley's comet: Preliminary analysis. In *Proceedings 20th ESLAB Symposium on the exploration of Halley's comet ESA SP-250* (B. Battrick, E. J. Rolfe, and R. Reinhard, Eds.), pp. 349–352. ESA, Heidelberg.

Schiaparelli, G. V. 1867. Sur les Etoiles Filantes, et specialement sur

l'identification der Orbites des Essaims d'Aout et de Novembre avec celles des Cometes de 1862 et de 1866. *Comptes Rendus* **64,** 598–599.

Sekanina, Z. 1974. Meteoric storms and the formation of meteor stream. In *Asteroids, Comets and Meteoric Matter* (C. Cristescu, W. J. Klepczynski, and B. Milet, Eds.), pp. 239–267. Scholium Int., New York.

Sekanina, Z. 1981. Distribution and activity of discrete emission areas on the nucleus of periodic Comet Swift–Tuttle. *Astron. J.* **86,** 1741–1773.

Shajn, G. 1923. The disturbing action of the Earth on meteoric showers. *Mon. Not. R. Astron. Soc.* **83,** 341–344.

Shiba, Y., K. Ohtsuka, and J. Watanabe. 1993. Concentrated radiants of the Perseids outburst 1991. In *Meteoroids and Their Parent Bodies* (J. Stohl and I. P. Williams, Eds.), pp. 189–193. Astronomical Inst. Slovak Acad. Sci., Bratislava.

Simek, M. 1987. Perseid meteor stream mean profile from radar observations in Czechoslovakia. *BAC* **38,** 1–6.

Southworth, R. B. 1963. Dynamical evolution of the Perseids and Orionids. *Smith. Contr. Astrophys.* **7,** 299–303.

Spurny, P. 1995. EN photographic Perseids. *Earth, Moon, Planets* **68,** 529–537.

Steel, D. I. 1994. Meteoroid streams. In *Asteroids, Comets, Meteors 1993* (A. Milani, M. Di Martino, and A. Cellino, Eds.), pp. 111–126. Kluwer Academic, Dordrecht.

Steel, D. I., and W. G. Elford 1986. Collisions in the Solar System. III—Meteoroid survival times. *Mon. Not. R. Astron. Soc.* **218,** 185–199.

Svorn, J., L. Neslusan, and V. Porubcan 1997. Determination of the period of activity of meteoroid streams. *Planet. Space Sci.* **45,** 557–562.

Twining, A. C. 1862. On meteoric rings as affected by the Earth. *Am. J. Sci.* **32,** 244–258.

Verniani, F. 1973. An analysis of the physical parameters of 5759 faint radio meteors. *J. Geophys. Res.* **78,** 8429–8462.

Whipple, F. L. 1951. A comet model II. Physical relations for comets and meteors. *Astron. J.* **113,** 464–474.

Whipple, F. L. 1980. Rotation and outburst of Comet P/Schwassman–Wachman 1. *Astron. J.* **85,** 305–313.

Whipple, F. L., and F. W. Wright 1954. Meteor stream-widths and radiant deviations. *Mon. Not. R. Astron. Soc.* **114,** 229–231.

Williams, I. P. 1993. The dynamics of meteoroid streams. In *Meteoroids and Their Parent Bodies* (J. Stohl and I. P. Williams, Eds.), pp. 31–41. Slovak Academy of Sciences, Bratislava.

Williams, I. P. 1996. What can meteoroid streams tell us about the ejection velocities of dust from comets? *Earth, Moon, Planets* **72,** 321–326.

Williams, I. P., and Z. Wu 1994. The current Perseid meteor shower. *Mon. Not. R. Astron. Soc.* **269,** 524–528.

Wu, Z., and I. P. Williams 1993. The Perseid meteor shower at the current time. *Mon. Not. R. Astron. Soc.* **264,** 980–990.

Yau, K. C. C., D. Yeomans, and P. R. Weissman 1994. The past and future motion of Comet P/Swift–Tuttle. *Mon. Not. R. Astron. Soc.* **266,** 303–316.